IOWA STATE UNIVERSITY
Digital Repository

Retrospective Theses and Dissertations

Iowa State University Capstones, Theses and Dissertations

2003

# Waveguides in three-dimensional photonic bandgap structures

Curtis Friedrich Sell
*Iowa State University*

Follow this and additional works at: https://lib.dr.iastate.edu/rtd

 Part of the Electrical and Electronics Commons

Recommended Citation
Sell, Curtis Friedrich, "Waveguides in three-dimensional photonic bandgap structures " (2003). *Retrospective Theses and Dissertations*. 617.
https://lib.dr.iastate.edu/rtd/617

This Dissertation is brought to you for free and open access by the Iowa State University Capstones, Theses and Dissertations at Iowa State University Digital Repository. It has been accepted for inclusion in Retrospective Theses and Dissertations by an authorized administrator of Iowa State University Digital Repository. For more information, please contact digirep@iastate.edu.

www.manaraa.com

# INFORMATION TO USERS

This manuscript has been reproduced from the microfilm master. UMI films the text directly from the original or copy submitted. Thus, some thesis and dissertation copies are in typewriter face, while others may be from any type of computer printer.

The quality of this reproduction is dependent upon the quality of the copy submitted. Broken or indistinct print, colored or poor quality illustrations and photographs, print bleedthrough, substandard margins, and improper alignment can adversely affect reproduction.

In the unlikely event that the author did not send UMI a complete manuscript and there are missing pages, these will be noted. Also, if unauthorized copyright material had to be removed, a note will indicate the deletion.

Oversize materials (e.g., maps, drawings, charts) are reproduced by sectioning the original, beginning at the upper left-hand corner and continuing from left to right in equal sections with small overlaps.

ProQuest Information and Learning
300 North Zeeb Road, Ann Arbor, MI 48106-1346 USA
800-521-0600

# Waveguides in three-dimensional photonic bandgap structures

by

Curtis Friedrich Sell

A dissertation submitted to the graduate faculty

in partial fulfillment of the requirements for the degree of

DOCTOR OF PHILOSOPHY

Major: Electrical Engineering (Microelectronics)

Program of Study Committee:
Gary Tuttle, Major Professor
Kai-Ming Ho
Vikram Dalal
Rana Biswas
Robert Weber

Iowa State University

Ames, Iowa

2003

UMI Number: 3085943

UMI®

UMI Microform 3085943

Copyright 2003 by ProQuest Information and Learning Company.
All rights reserved. This microform edition is protected against
unauthorized copying under Title 17, United States Code.

ProQuest Information and Learning Company
300 North Zeeb Road
P.O. Box 1346
Ann Arbor, MI 48106-1346

**Graduate College**
**Iowa State University**

**This is to certify that the doctoral dissertation of**

**Curtis Friedrich Sell**

**has met the dissertation requirements of Iowa State University**

Signature was redacted for privacy.

**Major Professor**

Signature was redacted for privacy.

**For the Major Program**

# TABLE OF CONTENTS

## ABSTRACT

This dissertation examines fundamental characteristics of photonic crystal waveguides. After taking a look at traditional waveguides and the history of photonic bandgap crystals, we examine different types of photonic bandgap crystal-based waveguides. We measure the frequency response of several waveguide designs for tightly confined waves. We connect our waveguides to the external world by using coupling probes. We also consider coupling using embedded horns, a method suitable for optical wavelengths.

A photonic bandgap crystal is a structure that does not allow waves of certain frequencies to propagate. This frequency range extends from 11.2 to 13.3 GHz for microwaves in the K-band for the crystal used here. Waveguides are formed by introducing line defects into the crystal.

After examining coupling we look at additional waveguide topics: waveguide bends, waveguide transmission loss, and waveguide dispersion spectra. These topics allow us to move towards a deductive design approach for photonic waveguide circuits, away from the cut-and-try approach commonly practiced up to this point. Mode mapping allows us to compare transmission matrix theory to our results. We found agreement in the shape of the modes, but a slight shift in frequency and propagation vector.

All of the photonic waveguide structures presented here were built from a single ceramic dielectric as well as air. This makes the structures fundamentally scalable to optical wavelengths. We gain knowledge on how to construct useful waveguides once we have the capability to make photonic crystal waveguides at these wavelengths.

# CHAPTER 1. INTRODUCTION

The purpose of this investigation was to study waveguides in photonic bandgap crystals. Let me begin with a brief definition of waveguides and photonic bandgap crystals.

A waveguide allows one to control electromagnetic waves, such as light or microwaves. It guides the electromagnetic waves from their source to a desired destination. A fiber optical cable is an example of such a waveguide.

A photonic bandgap (PBG) crystal is a structure built from a dielectric material, such as glass.[1] However, in this study a ceramic material is used, which has a higher dielectric constant than glass. The PBG crystal used here repeats in three dimensions as shown in Figure 1.1. PBG structures do occur in nature, for example, in the form of opal, a semiprecious stone.[2] In all three cases waves are reflected due to a photonic bandgap, which thus is responsible for the colors seen.

A PBG crystal is transparent for waves of most wavelengths, but

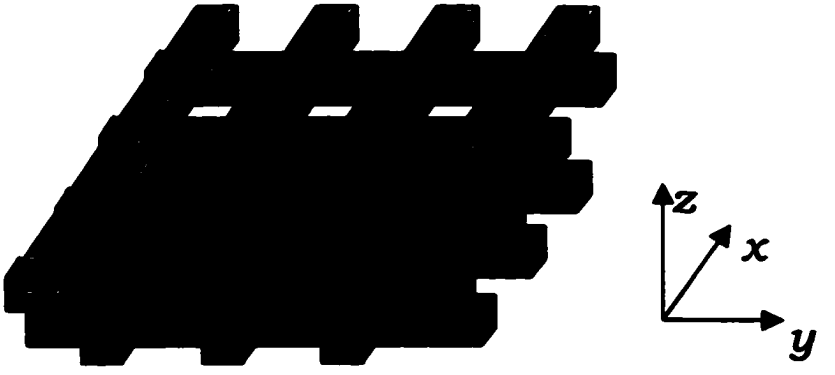


Figure 1.1: Four layers of a layer-by-layer photonic bandgap crystal. The stacking sequence repeats after four layers. A coordinate system is shown for reference.

waves of certain wavelengths cannot penetrate the PBG crystal. They are reflected instead. The frequencies corresponding to these wavelengths are referred to as the photonic bandgap of this crystal.

A photonic bandgap crystal can be used to construct a PBG waveguide. In principal, if one could simply drill a large hole through the crystal, waves entering this hole would be forced to follow its twists and turns: They would be guided.

One may wonder at this point why photonic crystal waveguides are of interest. After all, traditional waveguides exist, which are suitable for many applications. Metallic waveguides and dielectric waveguides come to mind. There are also some structures that combine features of metallic and dielectric waveguides, such as the microstrip lines used on electrical circuit boards.

Metallic waveguides are limited in their upper useful frequency. For frequencies above 100 GHz, the surface of the metal is no longer a perfect mirror and a small percentage of the impinging wave is absorbed. For example, aluminum at optical wavelengths loses 8% of the incident light and reflects the rest.[3] While this is not a problem in regular mirrors, it is in waveguides. A wave traveling in a waveguide undergoes many reflections, and the losses add up, making the waveguide suitable only for short distances.

Dielectric waveguides suffer from a different loss mechanism. Waves travelling in a dielectric waveguide are contained primarily within the dielectric material. These waves hit the surface of the dielectric material at a grazing angle and are reflected, due to total internal

reflection. If the waveguide is bent, the incidence angle of the light onto the dielectric's surface changes. If the waveguide is bent around a corner a small amount of the incident wave is no longer reflected: It leaks out of the waveguide, causing losses. Of course, such losses can be minimized by avoiding sharp bends.

A photonic bandgap crystal waveguide combines the advantages of metallic and dielectric waveguides. The PBG waveguides discussed here are built from dielectric rods, which eliminates the losses associated with metallic structures. PBG waveguides do not rely on total internal reflection but on interference to contain the waves within the waveguide. Thus it becomes possible to have sharp bends without the losses seen in dielectric waveguides or in metallic waveguides at high frequencies. For these reasons PBG waveguides have become a topic of interest.

The structure used here was chosen because it exhibits a broad bandgap and a high attenuation within the bandgap. It is also comparatively easy to construct and study. All of the measurements discussed were made using microwaves from 10 to 15 GHz in the K-band. These waves have a wavelength in the 3-cm range.

Waveguide types traveling in several directions were examined. The directions were chosen to enable the construction of a three-dimensional network of waveguides. The results of this work can be scaled to other wavelengths, due to the fundamental scalability of Maxwell's equations,[4] allowing the results to be used as design guidelines for future work.

PBG-based waveguides are prime candidates for use as interconnects in all optical integrated circuits. Other applications include

fiber optical communication, in particular channel drop filters or directional couplers.

To place this work in a broader context I looked at other work done on PBG waveguides. Sigalas et al.[5] predicted high transmission coefficients through Type X waveguides. Type X waveguides are constructed by removing a single rod from the PBG crystal, as shown in Figure 1.2. Their predictions were based on finite difference time domain simulations. The predicted loss remained low even for sharp bends.

Chutinan and Noda[6] made similar predictions, also based on finite difference time domain simulations. In addition, they noted that the loss for waveguide bends in crystal slabs of three lattice constants in thickness did not differ significantly from bends in thicker slabs. Although they pointed out the possibility of other waveguide designs, they presented few results.

Bayindir et al.[7] presented experimental data on beam splitters. Once again, a Type X waveguide was used. The paper presented frequency response graphs and claimed close agreement with Chutinan

Figure 1.2: A rod has been removed from this photonic crystal. This opens a waveguide, indicated here by an arrow.

and Noda's simulation results.

Finally, Kavanaugh[8] presented a simple theoretical model and measurements for a Type X waveguide. He noted difficulties in getting a wave to couple into the waveguide. While observing transmission, he did not draw conclusions about the waveguide's frequency response or transmission efficiency.

In chapter two, I present an overview of photonic bandgap crystals. I examine the different types of photonic bandgap crystals, which are periodic in two or three dimensions. Chapter Three discusses traditional waveguides. A familiarity with them is useful when examining PBG waveguides.

All of the papers mentioned above focused on examining Type X waveguides. A systematic examination of other possible waveguides and their properties has not been performed. Chapter Four is aimed at filling this gap. It presents a survey of designs for photonic crystal waveguides and the frequency responses of these waveguides.

Chapter Five discusses coupling structures used to get radio waves into the waveguides. To use PBG waveguides we have to launch electromagnetic waves into them. Chapter Six presents networks of multiple waveguides, such as waveguide bends. In chapter Seven I discuss measurements that allow loss to be estimated for the Type X waveguide. Finally, in Chapter Eight I discuss dispersion measurements, which allow one to find the modes propagating in a waveguide.

# CHAPTER 2. PHOTONIC BANDGAP CRYSTALS

## Overview

A photonic bandgap crystal, also called a photonic crystal, is a periodic structure designed to manipulate the propagation of electromagnetic waves. Photonic bandgap structures can be found in nature. The best known example is opal, a semiprecious stone.[2] Light of frequency within the opal's photonic bandgap is reflected, which causes the stone to appear colorful, despite its being made of transparent silicon dioxide. The photonic bandgap edges in an opal shift as a function of direction, causing it to change its apparent color based on illumination. Other examples of naturally occurring photonic bandgap structures are found in butterflies and animals such as the Sea Mouse, a small, furry-looking marine worm.[9]

Photonic bandgap crystals are typically made by taking a unit cell containing dielectric materials of differing indices of refraction, or metals, and repeating this unit cell to construct the crystal. Crystals that contain metal are commonly referred to as metallic photonic bandgap crystals. Crystals that do not contain any metal are referred to as dielectric photonic bandgap crystals.

Photonic bandgap crystals do not allow electromagnetic waves of a certain frequency range to propagate, regardless of the direction of propagation attempted. This frequency range is referred to as the photonic bandgap; this property gives the photonic bandgap crystal its name.

It is interesting to note that some of the terminology used to describe photonic crystals is similar to the terminology used for semiconductors. This comparison can be instructive for people familiar with semiconductor physics, but keep in mind that while photonic crystals control the flow of photons, semiconductor crystals control the flow of electrons. Multiple photons (being bosons) are allowed to occupy the same space, but multiple electrons (being fermions) are not allowed to do this. One can avoid confusion between semiconductor behavior and the behavior of photonic crystals by keeping this difference in mind.

**History**

Photonic bandgap crystals were originally proposed by Yablonovitch as a means to control the spontaneous emission of a semiconductor laser.[1] Spontaneous emission plays a fundamental role in limiting the performance of semiconductor lasers. Yablonovitch suggested that by placing the laser within a photonic bandgap crystal spontaneous emissions could be suppressed, thus improving the performance of the laser. Such a structure is shown in Figure 2.1.

In later research, Yablonovitch and Gmitter presented a face-centered cubic structure, for which they measured a photonic bandgap at microwave wavelengths.[10] This was one of 21 structures that Yablonovitch and Gmitter studied. All of the structures were of the same lattice type, and all used dielectric spheres, or dielectric voids.

Several papers[11,12,13] used a planewave expansion method to examine the photonic band structure in the dielectric structure proposed

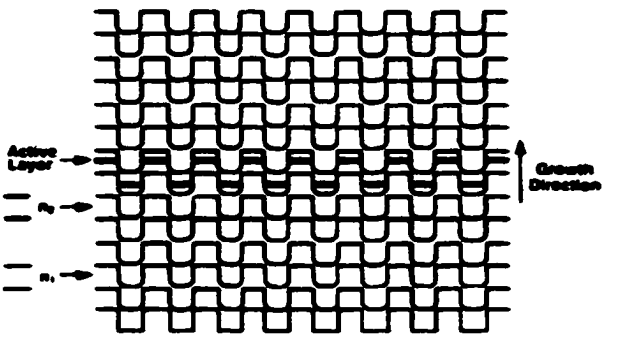

Figure 2.1: Side view of a photonic bandgap structure containing an active laser gain layer, as shown by Yablonovitch.[1]

by Yablonovitch and Gmitter. (Planewave expansion allows one to solve Maxwell's equations for a periodic dielectric structure of interest.) They found that this structure did not display a full photonic bandgap, but had a region with a low density of states, which was interpreted as a gap in the microwave measurements. This led Maddox to declare the demise of the photonic bandgap concept.[14]

Ho, Chan, and Soukoulis used the planewave expansion method to examine other lattice structures, and found that according to this model a diamond lattice structure should display a photonic bandgap.[13]

Yablonovitch, Gmitter, and Leung presented a structure with a face-centered-cubic lattice, seen in Figure 2.2, that displays a photonic bandgap.[15] The structure presented differed from prior designs in that the unit cell was no longer filled with a spherically symmetrical structure. Instead three intersecting cylindrical voids were used. The researchers used planewave expansion calculations as well as microwave measurements to confirm the presence of a full photonic bandgap.

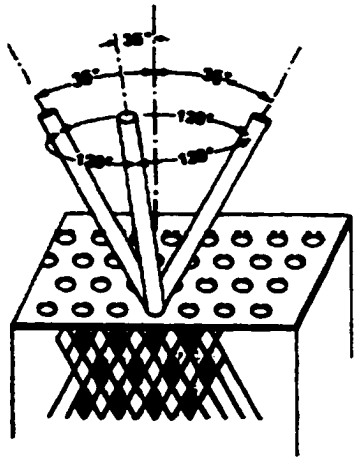

Figure 2.2: The face-centered-cubic photonic bandgap crystal proposed by Yablonovitch, Gmitter, and Leung. It can be made by drilling through a mask with a triangular array of holes into a block of material at three carefully chosen angles.[15]

Ho, Chan, Soukoulis, Biswas, and Sigalas presented a stacked-rod structure, which displayed a full photonic bandgap, and was suitable for microfabrication.[16] It is shown in Figure 2.3 and is similar to the structure used in this paper. They confirmed the photonic bandgap with planewave expansion calculations and microwave measurements.

**Two- and Three-Dimensional Crystals**

Photonic crystals are commonly classified by the number of their dimensions. The two main groups are two-dimensional photonic bandgap crystals and three-dimensional photonic bandgap crystals. The number counted is the number of dimensions that exhibit a photonic bandgap.

Occasionally one will find reference to one-dimensional photonic bandgap structures. A one-dimensional photonic crystal is repetitive along one direction, forming a stack of dielectric sheets. One-dimensional

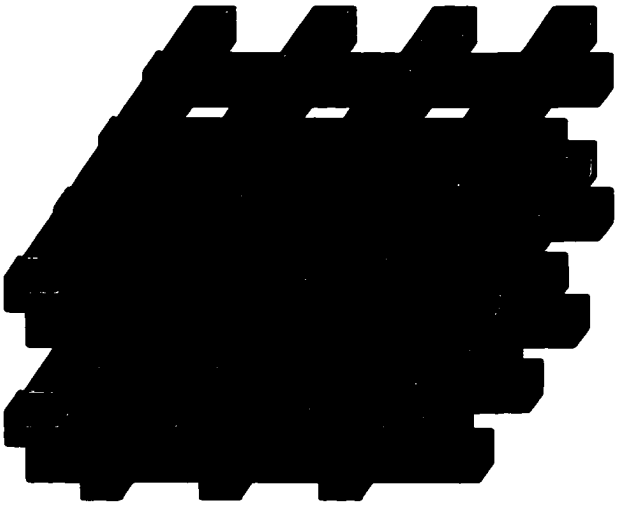

Figure 2.3: Layer-by-layer photonic bandgap crystal proposed by Ho, Chan, Soukoulis, Biswas, and Sigalas. This structure is built by orderly stacking dielectric rods.

photonic crystals are better known for their uses as interference filters or in Distributed Brag Reflectors.

**Two-Dimensional PBG Crystals**

Two-dimensional photonic crystals are structures that exhibit a photonic bandgap for waves travelling within a two-dimensional plane. There structures are periodic in this plane, which is often parallel to the substrate, but not in a direction perpendicular to this plane. An example of such a structure is an array of dielectric columns, as shown in Figure 2.4.

Two-dimensional photonic crystals are easy to construct for microwave wavelengths and can be made for shorter wavelengths using standard semiconductor processing techniques. To make a two-dimensional photonic bandgap crystal for optical wavelengths, one

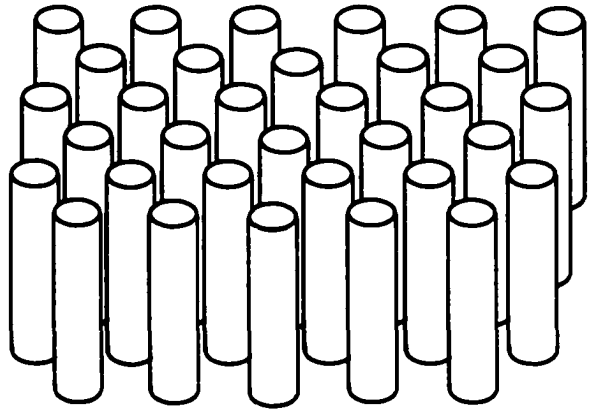

Figure 2.4: A structure with a two-dimensional photonic bandgap is formed by placing dielectric cylinders onto a square grid pattern.

patterns and etches a slab of material such that an array of either holes or pillars remains.

**Three-Dimensional PBG Crystals**

Three-dimensional photonic bandgap crystals are periodic in all directions and exhibit a photonic bandgap in all directions. A three-dimensional photonic bandgap crystal for K-band microwaves can be assembled from individual pieces of dielectric material, or they can be fabricated by drilling three sets of holes into a slab of material. (More detail regarding this will be discussed throughout this thesis as it becomes necessary.)

Photonic bandgap crystals are easy to make at K-band wavelengths, however, they presently remain difficult to fabricate for optical wavelengths.[17,18,19] This difficulty is due to the lack of a reversible or robust process. A reversible process is one that allows flaws to be corrected by undoing and redoing the processing step corresponding to

the flaw. While such rework is expensive, it is more economical than scrapping the flawed product. For example, if one layer in a stacked-layer photonic bandgap crystal turns out to be flawed, one may wish to remove and replace the flawed layer without starting over.

Another option is to find a robust process. Such a process would have a high yield (success chance) for individual layers, which is necessary to get a high yield for the finished crystal. To give a numerical example, let us assume a process with a yield for the individual layers of 95%. If we use this process to fabricate a 10-layer structure, we will have a yield of 60%. If we use this process to fabricate a 20-layer structure, we will have a 36% yield. Most of the structures, used in this work, had between 10 to 20 layers. We see that to get a reasonably high yield we need to have a very high success probability for the individual layers.

## Properties of the Crystal Used

### Physical Layout

For my research we used a photonic bandgap crystal built for centimeter-length microwaves, similar to the crystal described by Ho et al., shown in Figure 2.3.[16] we used alumina rods ($Al_2O_3$) with a measured dielectric constant of 3.0, a square cross section of 3.2 mm, and lengths from 15 cm up to 61 cm.

To form a layer these rods were placed in parallel with a center-to-center spacing of 10.9 mm. The sheets were stacked in a repeated four-step a-b-c-d sequence. The rods in the a and c layers ran parallel to each

other, as did the rods in the b and d layers. The rods in layer b ran perpendicular to the rods in layer a. The centers of the rods in layer c were shifted 5.4 mm from the centers in layer a. Similarly the centers in layer d were shifted in respect to layer b. The resulting crystal had a unit cell with a length and width of 10.9 mm and a height of four layers or 12.7 mm. (More detail on the construction of the crystal can be found in the Appendix.) Fill factor is the ratio of the dielectric-filled volume and the total volume. The final crystal had a fill factor of 29%.

**Microwave Behavior**

The completed structure had a measured photonic bandgap from approximately 11.2 to 13.3 GHz along the rods and from 10.4 to 15.7 GHz along the substrate normal. These measurements were taken with the crystal placed between a pair of horn antennas connected to a HP 8510 network analyzer, as seen in Figure 2.5. The measured transmission frequency response is shown in Figure 2.6.

The two observed cases are based on polarization: A wave propagating in the z-direction saw rods parallel to its electric field, but a wave propagating in the x- or y-direction was polarized in such a fashion

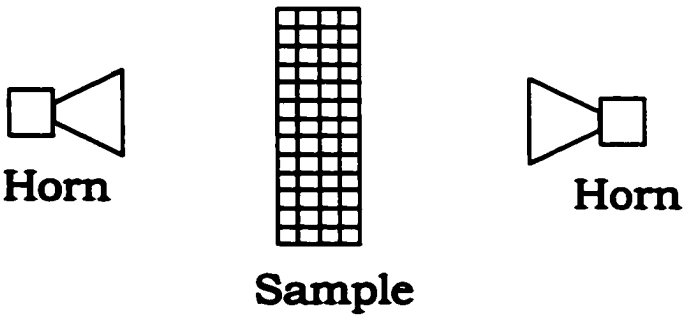


Figure 2.5: The photonic bandgap is measured with the crystal sample placed between a pair of horn antennas.

as to have no e-field component parallel to the rods. The measurement labeled "x or y" in Figure 2.6 was taken with the e-field perpendicular to the rods. If we were to take a measurement in the x- or y-direction for the case with the e-field parallel to the rods, we would observe a transmission spectrum very similar to the spectrum seen for the measurement along the substrate normal *z*.

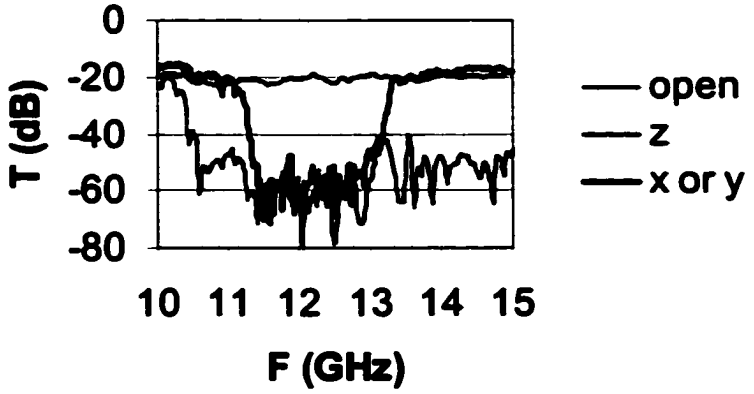


Figure 2.6: Transmission frequency response of a bulk layer-by-layer photonic crystal. "open" was measured without crystal, "z" was measured along the substrate normal, and "x or y" was measured in the substrate plane.

# CHAPTER 3. TRADITIONAL WAVEGUIDES

## Dielectric Waveguides

The two most common types of waveguide are dielectric and metallic. These two waveguide types differ substantially in their construction, their behavior, and their uses. In the following sections we will look first at dielectric waveguides and then at metallic waveguides. It is useful to study these waveguides for a comparison to PBG waveguides.

Dielectric waveguides are usually made from a dielectric material, as the name implies. This dielectric core is either surrounded by air or clad in a second dielectric layer with a smaller index of refraction than the core. Commonly used waveguides with a square cross section are discussed here, although circular and barrel-shaped cross sections are also frequently used.

Within a dielectric waveguide waves are guided by total internal reflection. Waves that hit the interface between two materials of differing index of refraction, such as air and glass, will be completely reflected if they are travelling in the medium with higher index of refraction and hit the interface at a grazing incidence angle. This can be observed by looking at the end of a clear glass rod. Viewed from an end, a glass rod looks like a silvery tube. The glass rod behaves like a large diameter optical fiber.

Dielectric waveguides are commonly used for frequencies above 30 GHz. The lowest order mode has no cutoff frequency. This means there is no minimum frequency required for a wave to travel along a dielectric

waveguide. Instead, for a given waveguide, longer wavelength waves occupy more of the space surrounding the waveguide.

**Metallic Waveguides**

Metallic waveguides are essentially tubes made from a metal, which has been selected to be highly reflective at the wavelength used. The metallic waveguides discussed here have a rectangular cross section. This is the type of cross section most frequently used, although the use of other cross sections is possible.

In a metallic waveguide waves are guided by reflection from the metallic walls. Metallic waveguides have a lower cutoff frequency: $f = c/2a$, where $c$ is the speed of light and $a$ is the width of the waveguide. The lower cutoff frequency is the lowest frequency that will allow propagation in a waveguide. A wave with a frequency below cutoff may still enter the waveguide, but it will not propagate. Instead it will decay exponentially as a function of distance along the waveguide.

Metallic waveguides are commonly used from 1 to 100 GHz. For frequencies above 100 GHz they become lossy due to nonperfect reflection from the metal walls at higher frequencies.

Metallic waveguides are used primarily for microwave applications; a common use is in microwave ovens. Here a metallic waveguide connects the magnetron, which generates the microwaves, to the cooking chamber.

# CHAPTER 4. PBG WAVEGUIDES

## Hollow Guides

In this chapter waveguides within a layer-by-layer photonic crystal structure are studied. First, waveguides of various types necessary for building three-dimensional networks were created by removing material from the photonic crystal. Next the waveguides' frequency responses were measured with a network analyzer, and finally the results were compared to numerical calculations based on a supercell technique using planewaves.

Waveguides can be formed within 2-D and 3-D photonic bandgap crystals by removing material. Waveguides are formed in 2-D structures by removing a row of rods thus forming a slot. Preventing energy leakage from these waveguides has been shown to be difficult.[20] Three-dimensional PBG waveguides are enclosed by the bulk crystal on all four sides, making them less leaky. For PBG-based waveguides and waveguide bends, losses lower than those for comparable metallic or dielectric waveguides have been predicted.[5] Three-dimensional waveguides present additional advantages: They can cross under each other, forming three-dimensional networks, and they can couple out of any surface of the crystal.

We examined waveguides in a stacked-rod structure. The structure studied here had its photonic bandgap in the K-band for microwaves. Since dielectric photonic crystals are scalable, the measurement results can be applied to photonic crystal waveguides operating at other wavelengths. The stacked-rod structure was chosen because it exhibits a

wide bandgap and high attenuation at midgap. It is also comparatively easy to construct and study. This chapter focuses on narrow waveguides, which have a low number of propagation modes.

Waveguides of three distinct types were examined here:[21] Type X, Type II Y, and Type II Z, shown in Figure 4.1. The type letter denotes the direction of the axis of the waveguide prototype. One property the waveguides shared was that all had been made by removing material from the crystal. The waveguide types differ in the lateral placement of the axis, the number of crystal layers occupied, and the number of symmetry planes. The properties of the waveguides are listed in Table 4.1.

The frequency response was measured using a HP 8510 network analyzer. To perform this measurement the crystal was connected to the 8510 test ports using coaxial cables. Signals were coupled into the PBG waveguide openings using capacitive coupling probes. These probes were fashioned out of the ends of the coaxial cables by exposing 14 mm of the center conductor and bending the last 8 mm into a loop. Losses in

Table 4.1: Properties of four waveguide types

| Waveguide Type | X | I Y | II Y | II Z |
|---|---|---|---|---|
| Constructed by removing | Entire rod | Rod pieces | Rod pieces | Rod pieces |
| Location | In 1 layer | In 1 layer | In 1 layer | Runs along stacking direction |
| Number of symmetry planes | 2 | 2 | 1 | 1 |
| Centered on | Rod | Rod in next layer | Gap between rods | Gap between rods |

coupling and the cables added up to about 25.5 dB. This coupling configuration was chosen for its flat and easily reproducible frequency response. The flat frequency response is due to the small size of the coupling probe, which is a fraction of a wavelength long.

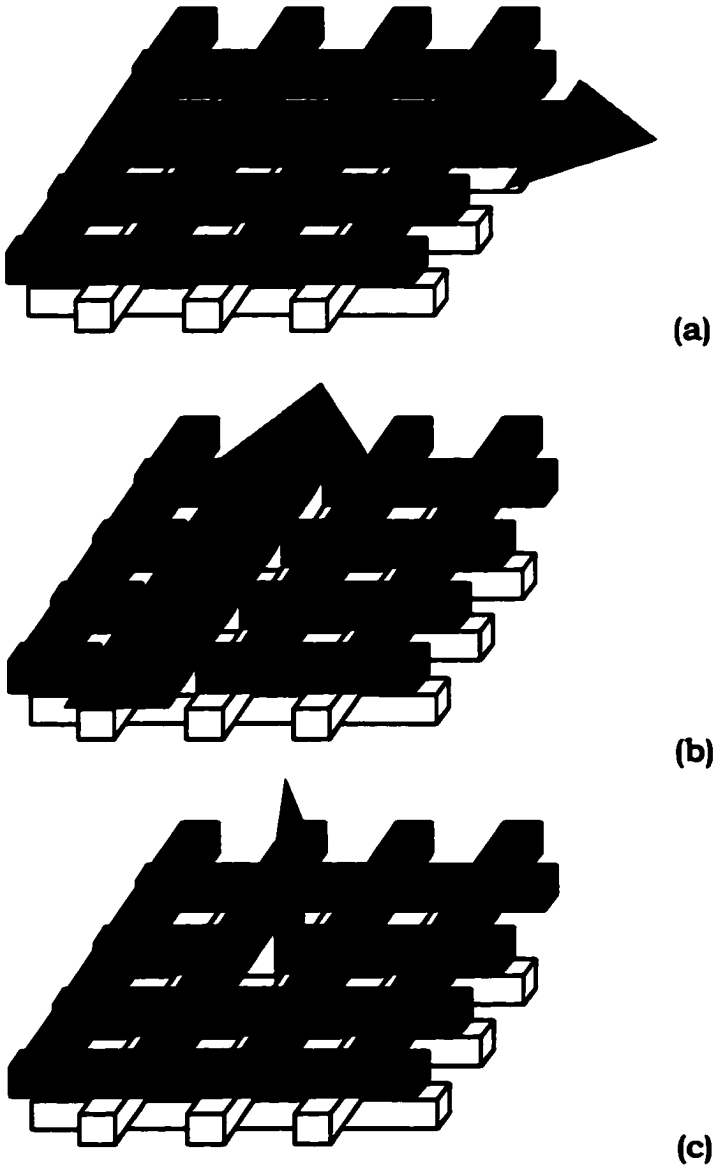


**Figure 4.1: Photonic crystal waveguides created by removing rods or rod sections. (a) Type X waveguide, (b) Type II Y waveguide, and (c) Type II Z waveguide. The waveguides are shown in small photonic crystal fragments.**

To avoid waveguide loss due to evanescent waves leaking through the bulk crystal to the waveguide surface, the waveguide had to be embedded in the bulk of the crystal, away from the top and side surfaces. To determine the minimum distance needed between the waveguide and the sides of the crystal, it is useful to look at waveguide loss as a function of distance to that edge, shown in Figure 4.2. It can be seen that the transmission loss decreases as the distance to the edge is increased; it reaches a plateau once the distance to the edge is greater than 2.5 lattice constants. Similar observations were made when the waveguide was moved in the z-direction. This agrees with theoretical calculations.[6] For the remaining measurements in this dissertation, waveguides were located three or more lattice constants (that is twelve layers) from the edges of the crystal.

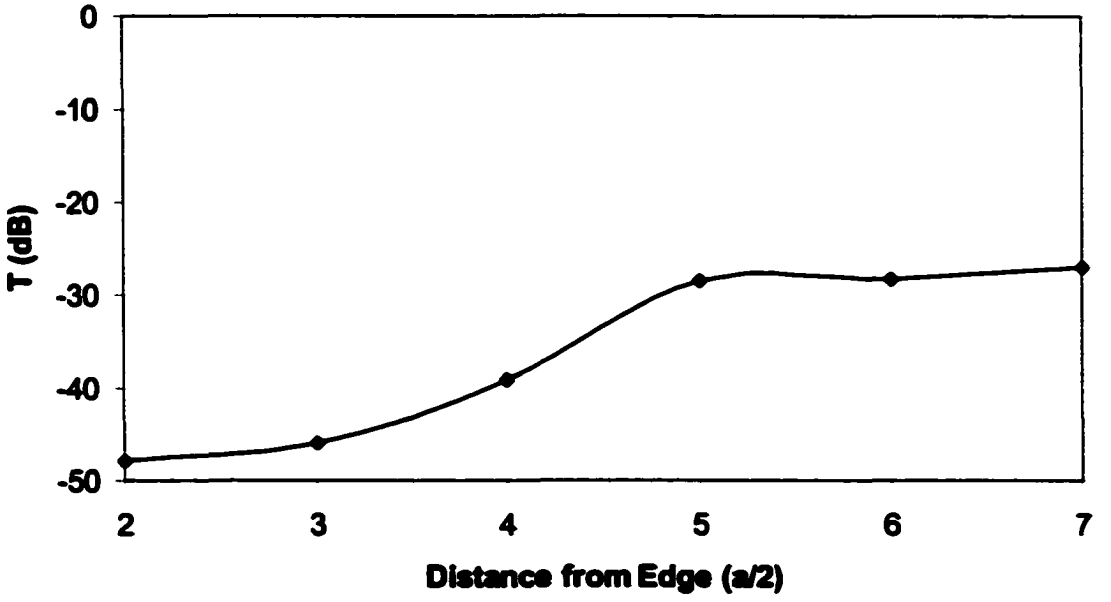


Figure 4.2: Graph of loss as a function of distance from edge for Type X waveguides.

Loss can also be measured as a function of length. This allows one to separate the loss due to coupling from the loss due to the length of the waveguide (Figure 4.3). This measurement was taken by incrementally increasing the length of the Type X waveguide between the coupling probes. Periodic ripples on the order of one-quarter of a lattice constant were observed. They were likely caused by the proximity of the coupling probe and the nearest rod in the y-direction. Coupling is at a maximum if the coupling probe is halfway between two rods. No global increase in loss as a function of length was observed; thus the waveguide displayed no appreciable loss in eight lattice constants. The sum of all the losses was approximately 25.5 dB, mainly due to the coupling probes and their coaxial cables.

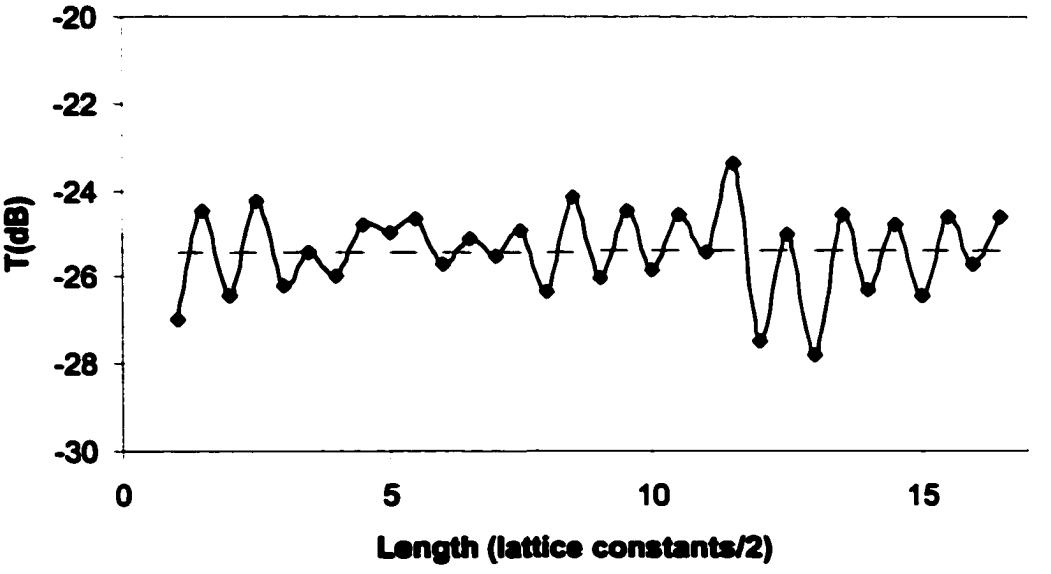


Figure 4.3: Loss as a function of length for Type X waveguides. The dashed line marks a root-mean-squared fit.

**Frequency Response**

Finally, it is of interest to study the frequency response of various waveguide types, as well as to study frequency response as a function of waveguide width. The same measurement setup as above was used. For the Type X waveguide, transmission within 10 dB of the peak was observed from 11.5 to 12.6 GHz (Figure 4.4). A dip in the transmission was observed for 12.4 GHz, indicating that two separate waveguide modes may be participating in the transmission. It was difficult to excite every mode simultaneously, since each mode required a different placement of the coupling probes. Theoretical simulations confirmed the presence of two modes.[21]

For Type Y waveguides, transmission was examined as a function of width. A waveguide of 11 lattice constants in length was used. The width of the waveguide was varied between measurements. The frequency of the

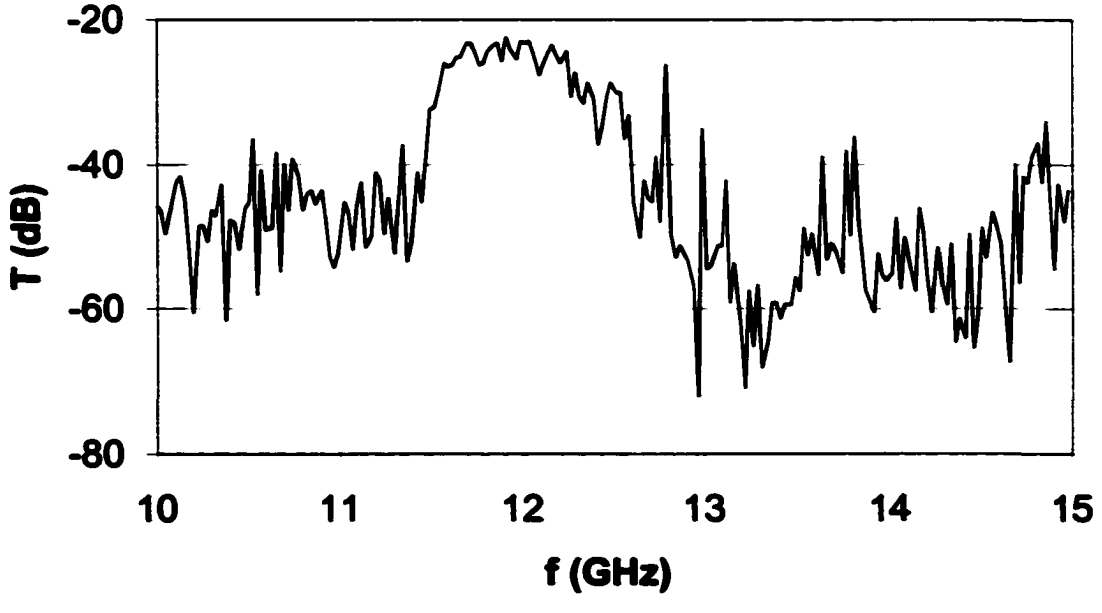


Figure 4.4: Transmission frequency response for a Type X waveguide.

upper transmission mode edge increased as a function of width (Figure 4.5). For waveguides with widths on the order of one or more lattice constants, additional modes can be observed. Simulations predict the presence of a single-mode for narrow Type II Y waveguides, and two overlapping modes for Type I Y waveguides. Overlapping modes allow

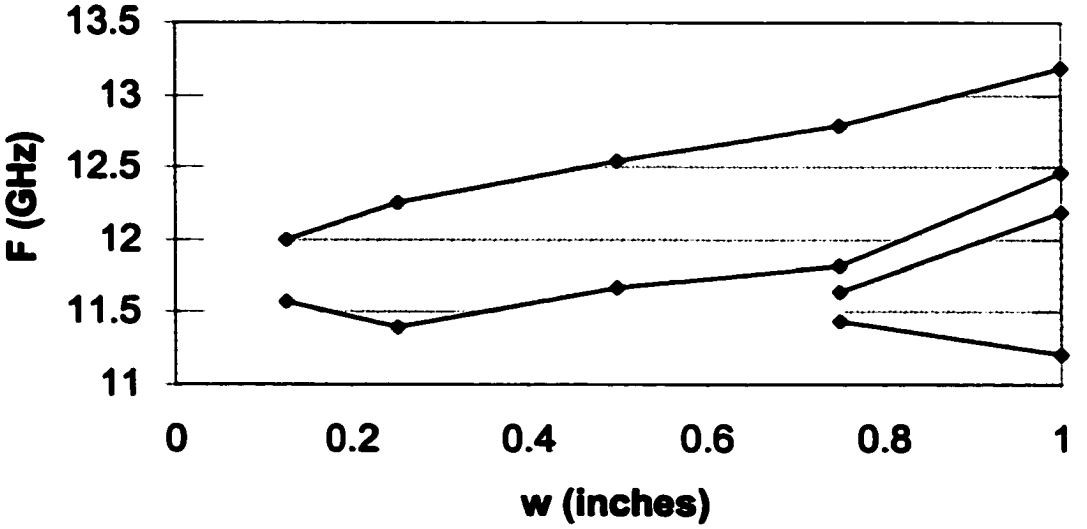


(a)

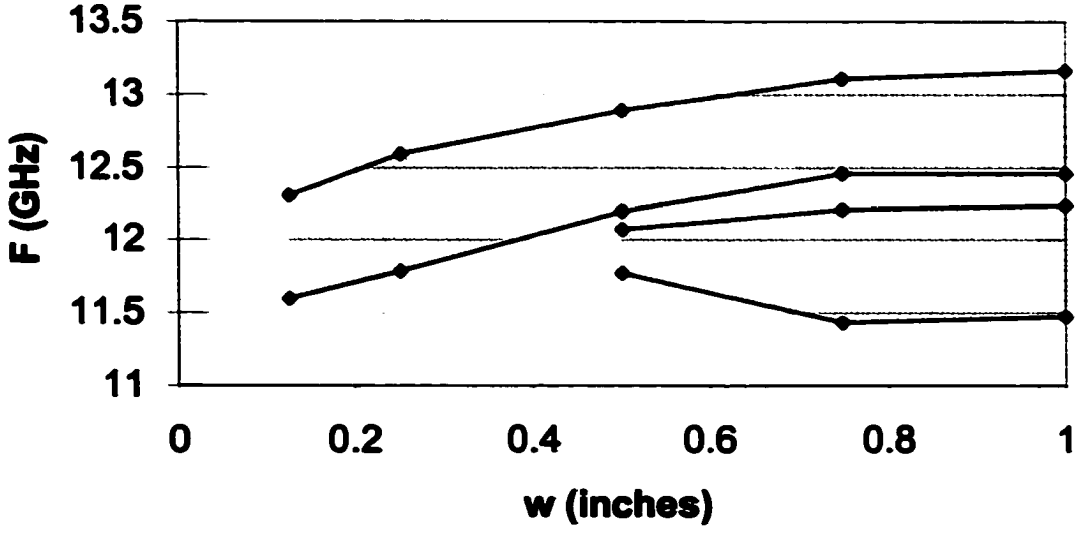


(b)

Figure 4.5: Type Y waveguide transmission as a function of width. a) Type I Y guide, b) Type II Y guide.

energy to be transferred between them. This complicates using Type I Y waveguides since it is difficult to effectively couple into both modes at the same time.

Transmission was also observed as a function of width in Type II Z waveguides. Type Z waveguides can be used as interconnects between layers of Type X and Type Y waveguides, or for coupling into the surface of the crystal. The waveguides used in these measurements were five lattice constants long. The center frequency of the transmission mode increases as a function of waveguide width, as well as the width of the transmission mode (Figure 4.6). Additional transmission modes were observed for widths on the order of and greater than one lattice constant. The number of modes agrees with the simulations.

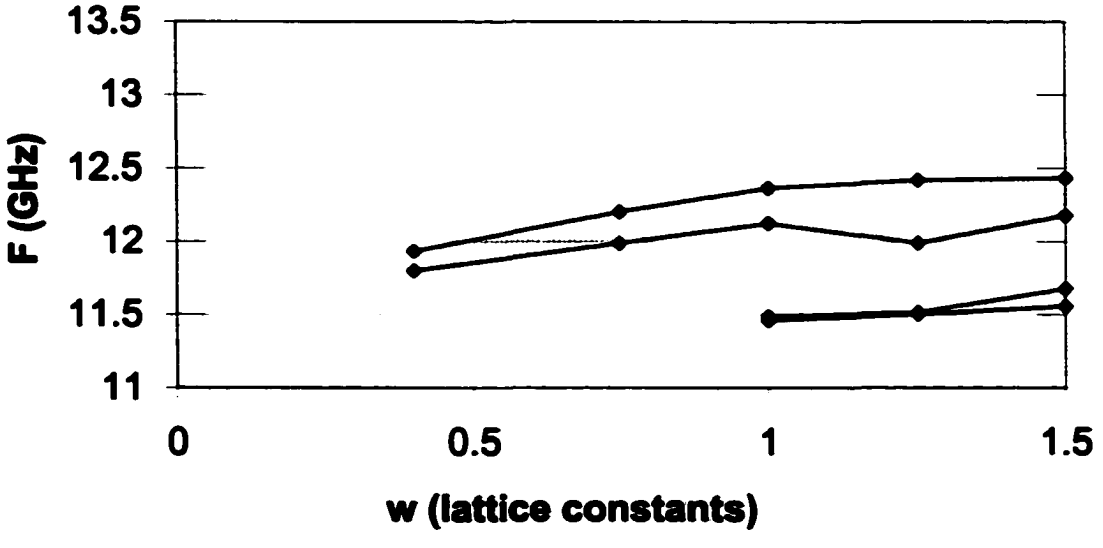


Figure 4.6: Type II Z waveguide transmission as a function of width.

**Filled Guides**

This research has mainly focused on waveguides built by removing material from a crystal. It is also possible to construct a waveguide by adding material to a crystal. So far we have ignored this possibility primarily due to a perceived problem of dissipative losses. The bulk of the dissipation takes place in the electric field antinodes, which are the points of maximum field strength. For a waveguide constructed by removing material, the antinodes are located in the air-filled core of the waveguide. This can be seen in propagation simulations.[5,6] Air is less lossy than most dielectric materials. Thus, by placing the antinodes in the air-filled region of the waveguide we minimize loss.

Despite being more lossy, filled waveguides have an interesting property. Modes in material-filled waveguides can be confined by two mechanisms: Reflection due to the photonic bandgap, and total internal reflection. Since total internal reflection does not rely on the photonic bandgap, a dielectric-filled waveguide can potentially guide waves at frequencies outside the photonic badgap, just like a dielectric waveguide.

To examine this possibility we built a dielectric-filled waveguide by adding a single rod centered in the gap between two existing rods of bulk crystal. This rod lies within a layer of the crystal and runs parallel to the other rods in that layer.

Three measurements are presented in Figure 4.7. The filled waveguide discussed above, a Type X waveguide constructed by removing a rod, and the bulk crystal without any waveguide are shown. All three

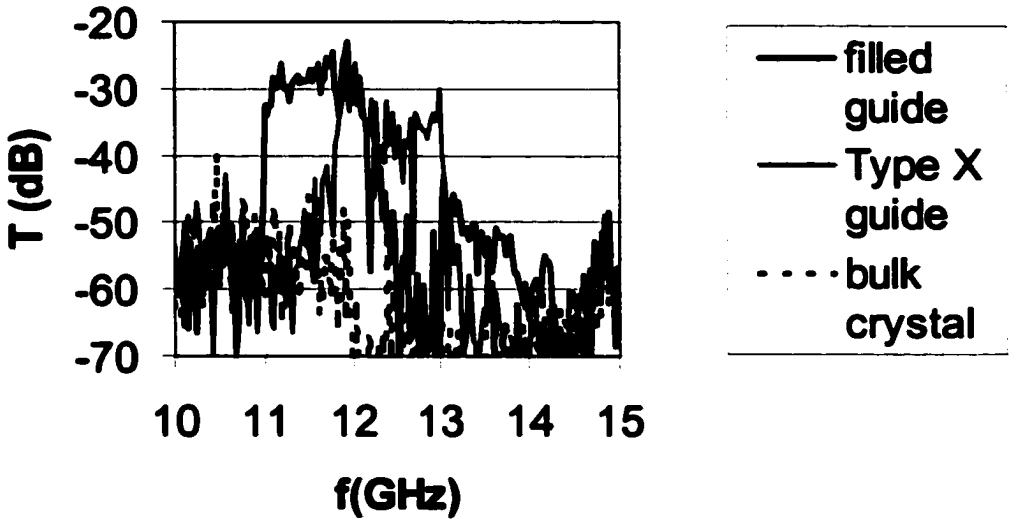


Figure 4.7: Measured frequency response of a filled photonic waveguide, with a Type X guide and the bulk crystal for comparison.

measurements were taken using metal horns placed 2 cm from the surfaces with the waveguide openings.

We observed guiding for frequencies from 11.0 to 12.1 GHz. For the waveguide presented here it was not clear if the transmission band extended below the bottom edge of the photonic bandgap. It should be possible to work more on this topic by examining waveguides filled with additional material. One could easily extend the above design to a waveguide filled with two rods.

**Waveguides in Two-Dimensional Photonic Crystals**

Waveguides can also be constructed in two-dimensional photonic bandgap crystals. Two types of waveguide are possible: Guides parallel to the rods in the z-direction, and guides perpendicular to the rods in the x-y plane. As shown in Figure 4.8, a guide parallel to the rods can be

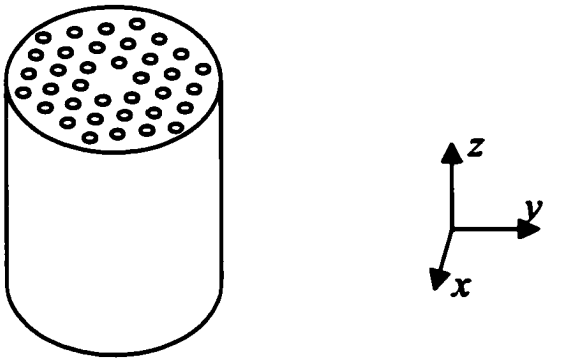


Figure 4.8: Photonic crystal fiber based on two dimensional photonic bandgap crystal. The center feature is missing. This creates a defect, which guides the light in the z-direction.

constructed by removing one rod. Guiding in the z-direction is of interest in optical fibers. Guides perpendicular to the rods can be constructed by removing a row of rods and using total internal reflection to keep the electromagnetic waves from leaking out of the top and bottom, as shown in Figure 4.9. Guiding in the x-y plane is of interest for on-chip interconnects.

The main advantage of waveguides in two-dimensional photonic crystals over other structures is that they are easy to fabricate. The main drawback is loss in sharp bends due to mode coupling. Creating cavities

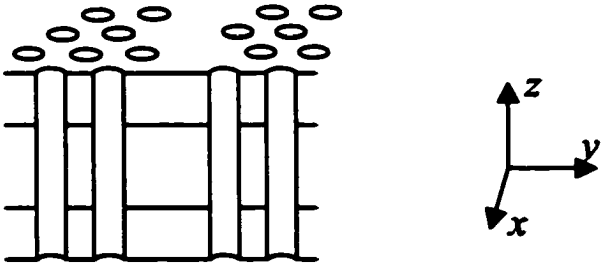


Figure 4.9: Waveguide created in a two-dimensional photonic crystal. A missing row of holes guides the waves in the x-direction. Total internal reflection is used to prevent waves from leaking in the z-direction.

**at the vertices of the bends or using gradual bends may overcome these losses.**

# CHAPTER 5. COUPLING INTO PBG WAVEGUIDES

To examine the propagation of waves within a photonic waveguide we need to couple waves into and out of the waveguide.

## Prior Work

J. Kavanaugh examined photonic waveguides as part of his dissertation.[8] He constructed a waveguide in a stacked-layer structure by removing a single rod. For his initial measurements, Kavanaugh illuminated one end of the waveguide with a planewave by using a horn antenna. He was able to observe transmission for only a narrow range of frequencies.

Kavanaugh also performed measurements using a tapered rod antenna to improve coupling. His tapered rod antenna was constructed with a square end, that fit snugly into the waveguide opening, and a tapered end. In theory, waves are able to couple from free space into the tapered end of the antenna, propagate along the length of the rod, and couple into the waveguide at the other end of the rod. Kavanaugh pointed out that ideally this second end should be tapered to a point, but he chose not to do so. This antenna improved coupling significantly and allowed Kavanaugh to observe a second narrow frequency transmission peak.

Examining waveguide transmission spectra presented by Bayindir et al., one notices fairly broadband transmission for waveguides constructed in a stacked-layer structure by removing a single rod.[7] Their paper describes measurements taken by illuminating one end of the waveguide with a planewave from a horn antenna, while using a second horn

antenna to observe the transmitted wave at the other end of the waveguide.

While the paper contains only a brief description of the experimental setup, I was able to learn additional details through personal discussions with Bayindir. To couple microwaves into the waveguide Bayindir placed horn antennas two centimeters from the face of the crystal. He inserted 2 to 4 cm alumina stubs into the opening of the waveguide to enhance coupling. The stubs were identical in material and cross section to the rods used for constructing the crystal. Each inserted stub worked as a coupling structure for a narrow frequency range. Larger frequency bands were covered by inserting multiple stubs.

Using ceramic stubs for coupling can be difficult. Each stub couples a narrow range of frequencies, based on its length and placement. Thus one has to select and place multiple stubs to reliably couple into a waveguide over the entire frequency range of interest. This places high demands on the experimenter due to the difficulty of observing the effects of stub placement independent of the waveguide transmission spectrum.

**Design Considerations**

An ideal coupling structure would combine a number of characteristics. Foremost it should have a reproducible transmission function, which is preferably a constant function of frequency. It should be easy to build and easy to use. Finally it should have an acceptable gain and be small in size. This may mean using separate structures, depending on the waveguide type being coupled into.

Considering the desired use of the coupling structure, one can make trade-offs. If primarily intended for microwave measurements, one can relax the requirements on size, ease of construction, and gain in favor of a reproducible transmission function and ease of use.

For optical applications we have to additionally consider coupling into the top surface of a crystal, rather than at an edge. This is due to an assumption that optical wavelength crystals will have a large top surface in a plane parallel to the substrate, but a small number of layers, thus leaving little surface along the other crystal edges. Ideally the coupling structure can be built in the same patterning steps that define the waveguides.

Examining the fields presented in photonic waveguide simulations[5,6] suggests it may be possible to couple into a waveguide by inserting an electrical probe into one of the nodes of the field. Such a design would be similar to the probes used for coupling into metallic waveguides.

**Coupling Probes**

The simplest coupling structure is a coupling probe. Many of the measurements presented here were taken using coupling probes. These probes were built using a length of 2.8-mm diameter coaxial cable, as shown in Figure 5.1. The insulation and the shield are stripped from the probe end of the cable, exposing a 14-mm length of the center conductor. The end of the center conductor is bent into a 2- to3-mm loop, which is soldered shut.

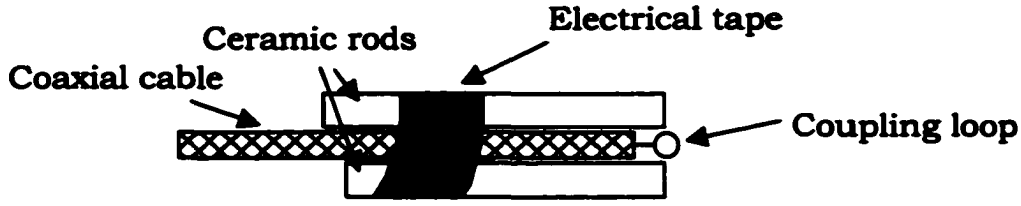


Figure 5.1: Diagram depicting the construction of a coupling probe. The ceramic rods are secured to the coaxial feed line using electrical tape.

Two ceramic stubs are taped to the outside of the cable, so that their ends line up with the center of the loop. The length of these rods is noncritical since their primary function is to prevent waves from leaking along the shield of the cable, as well as to provide mechanical stability. Small rod segments of 3 to 5 cm length, left over from building the crystal were used.

This probe is similar to Yablonovitch and Gmitter's monopole antenna, which had a 6-mm pin above a ground plane outside a bulk crystal to map the crystal's band diagram.[10] Differences between the probes used by Yablonovitch and Gmitter and those used here are the addition of a closed loop, which functions as a capacitive tophat to improve coupling, and the addition of the dielectric rods to reduce leakage.

Measuring the transmission frequency response of a Type X waveguide is a good test of the coupling probe's performance, due to the availability of experimental[7] and simulation[6] results. The recorded transmission response, shown in Figure 5.2, has the expected shape. The pass band is over 30 dB above the stop band noise. The transmission is reasonably flat, with no surges and only a few dips.

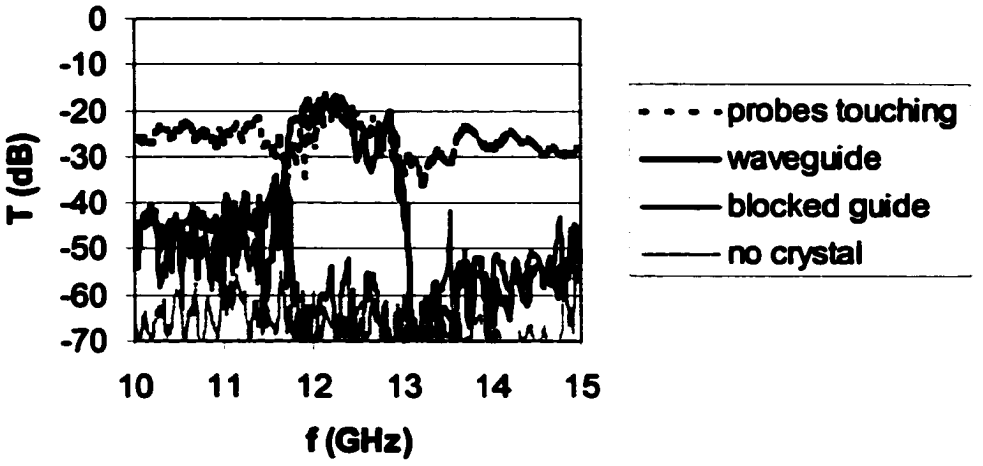


Figure 5.2: Frequency response of Type X guide, measured with coupling probes. Additional traces are shown for coupling probes touching each other within the crystal, a measurement with the probes stuck in a bulk crystal, and a measurement taken with the probes in free space, marked "no crystal".

The transmission response recorded matches well with the theoretical predictions made by Chutinan and Noda, and is in general agreement with the experimental results presented by Bayindir et al.

In Figure 5.2 we have shown additional measurement results. A measurement taken for a blocked waveguide shows no transmission, as expected. This measurement was recorded to ensure that there is no leakage path, for example, along the outside surface of the crystal.

The transmission measurement taken with both probes touching inside the waveguide gives an indication of the magnitude of the coupling loss. This loss is 12.7 dB per probe. A more accurate measurement was performed by systematically varying the waveguide length; it is presented in Chapter 7 on waveguide loss.

The coupling probes presented here do have limitations. They are lossy. This loss is acceptable for the measurements presented here, although it decreases the signal-to-noise ratio. The probes used contained metal, which is not a problem at the microwave frequencies used; it does, however, make the probe design unsuitable for optical wavelengths. Finally, the probe presented is best suited for Type X and Type Y waveguides, and can be used only in modified form for Type Z waveguides.

**Coupling PBG Horns**

In this section we examine frequency response, loss, and radiation pattern for horn antennas constructed into the surface of a photonic crystal. These horns are built by omitting material during the crystal's construction or by removing material from a finished crystal. The horns can be used to couple electromagnetic waves into waveguides contained within that crystal and are of a design suitable for optical frequencies. The horns presented here couple into waveguides running parallel to the surface into which the horns are embedded.

We present and examine photonic crystal-based horns for coupling electromagnetic waves into waveguides embedded within a stacked-layer photonic bandgap crystal.[7,16] The horns were constructed and tested in an easy to use centimeter scale. Ceramic dielectric material was used throughout the construction, allowing us to avoid lossy metals and making the results scalable in frequency. Thus the knowledge gained can be used for designs at optical wavelengths.

We investigate horns because they have a number of desirable properties. Horns can be built from the same dielectric materials as the bulk of the photonic crystal. Horns should be easy to construct since they can be fabricated in the same steps as the crystal. They can be built with large openings and broad radiation patterns, thus simplifying the alignment between photonic crystal components and other components (such as optical fibers) in a system. The horns presented here couple through the "top" surface of the crystal (parallel to the substrate), thus opening up the largest surface of the crystal for coupling. Finally, the horns couple into waveguides made by removing a single rod from the crystal. This is the best understood waveguide design for stacked-layer structures.

The photonic bandgap crystal used here was constructed in a layer-by-layer fashion.[16] Square alumina rods of 3.2-mm width and with a measured index of refraction of 3.0 were organized as shown in Figure 5.3. This photonic crystal has a filling ratio of approximately 29%, and a three-dimensional photonic bandgap extending from 11.2 to 13.3 GHz. The crystal used was 4.5 lattice constants thick (that is, 18 layers), 14 lattice constants wide, and 56 lattice constants long (6.4 cm * 15.2 cm * 61 cm long). Removing a single rod from this photonic crystal opens a highly confined waveguide[5,6] for frequencies from 11.5 to 12.6 GHz. We place the crystal in a Cartesian coordinate system, such that the substrate lies in the x-y plane and the waveguide runs in the x-direction. All of the horns we examine here point in the *z*-direction.

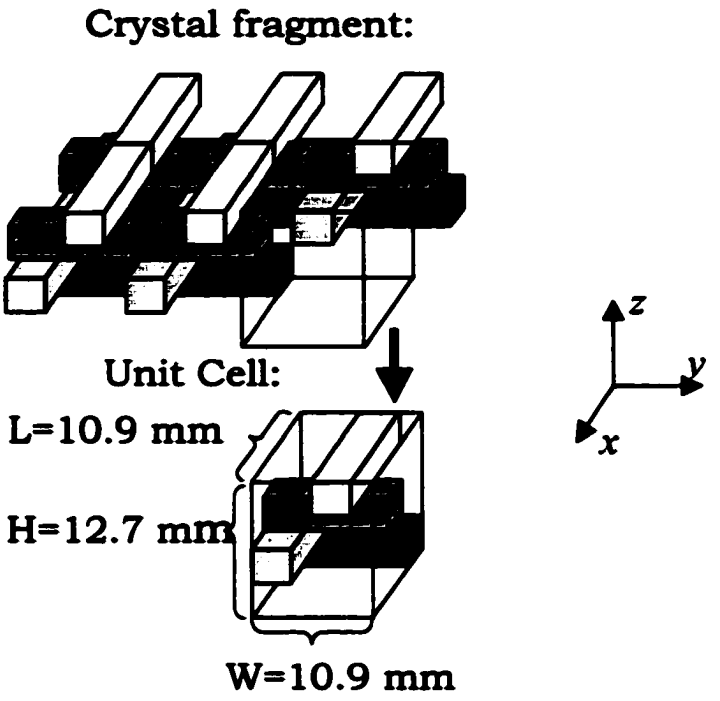


Figure 5.3: Schematic configuration of the fabricated 3-D layer-by-layer photonic crystal and its unit cell.

When designing the horn, we first need to consider which rods to remove. The horn will penetrate several layers of rods, which alternate between rods running in the x-direction and rods running in the y-direction, as seen in Figure 5.4. We can choose between removing rods of one direction only to form a horn, or removing rods in both directions. Some fabrication processes may favor removing only alternate layers of rods to reduce the number of masks, or removing rods in all layers for structural reasons.

We made this choice by examining the coupling at the bottom of the horn. To an electromagnetic wave the very bottom of the horn looks like a waveguide in the z-direction. We examined these waveguides using two coupling probes and found that we needed to remove rod segments

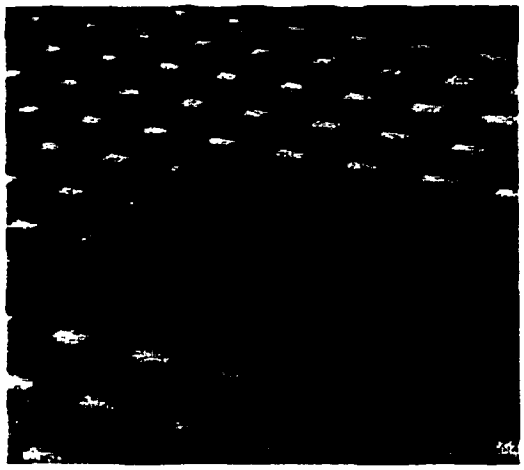

(a)

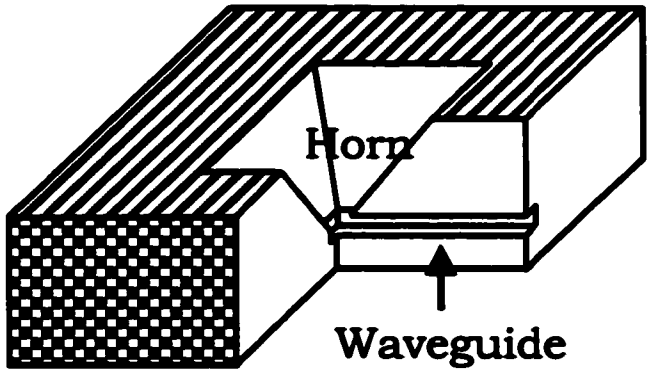


(b)

Figure 5.4: Photonic crystal horn integrated into the surface of the crystal. It is used for coupling into a photonic crystal waveguide. Part a shows a photograph of the completed photonic crystal horn; part b depicts the cross section of the horn and the waveguide. The photo was taken from the same point of view as the drawing in part b.

parallel to the guide's axis for optimum coupling. We can remove rods running in the x-direction only or we can remove all rods.

To study the two choices we built and compared two horns. Both were 8-layers (two lattice constants) tall. Frequency response was measured by coupling microwaves into the waveguide with a coupling probe, as seen in Figure 5.5. Waves radiating from the photonic crystal horn were detected with a Narda 639 standard-gain metal horn mounted

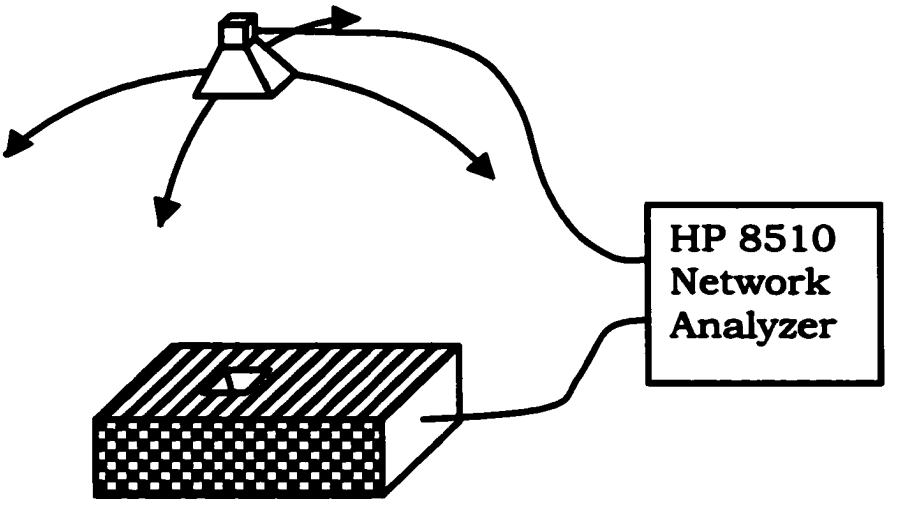


Figure 5.5: Experimental setup for measuring the frequency response and the radiation pattern of a photonic crystal horn. A metal horn can be moved in an arc in the x- or y-direction around the photonic crystal.

25-cm above the crystal. The metal horn could be moved in a 25 cm arc in the x- or y-direction for measuring the radiation pattern. A HP 8510 network analyzer was used to record the frequency response.

The results of the frequency response measurements for the comparison between a horn with alternate layers of rods removed and a horn with all layers of rods removed are shown in Figure 5.6. Both frequency responses were similar. This meant we could choose the design best suited to the fabrication process we would use. For the remainder of this work we will focus on horns that require only modifying alternate layers. At microwave frequencies these horns were easier to build than the other design.

Next we studied the effect of horn size on the transmission spectrum. We took measurements for horns that were 2, 4, 6, and 8 layers of rods tall. The results are shown in Figure 5.7. Going from 2 to 8

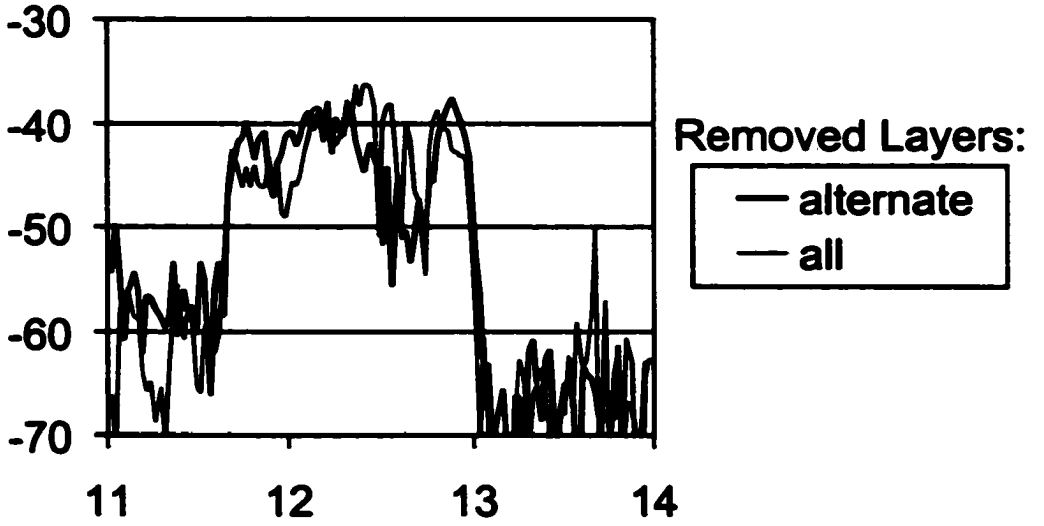


Figure 5.6: Comparison of the frequency response for a photonic crystal horn built by removing rods in alternating layers only and a photonic crystal horn built by removing all the layers of rods.

layers, a large dependence of transmission amplitude on horn size was seen. There was little improvement in transmission amplitude past 8 layers. This improvement was primarily due to a narrowing of the radiation pattern, which we will examine next.

Figure 5.8 shows the radiation patterns in the x- and y-directions

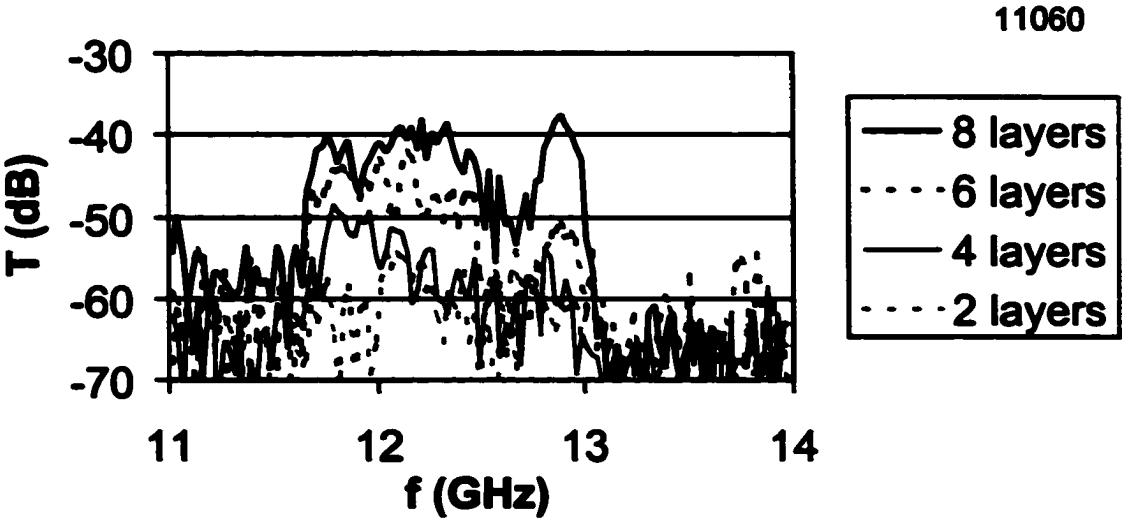


Figure 5.7: Transmission as a function of the photonic crystal horn size. Size is varied from 2 layers up to 8 layers.

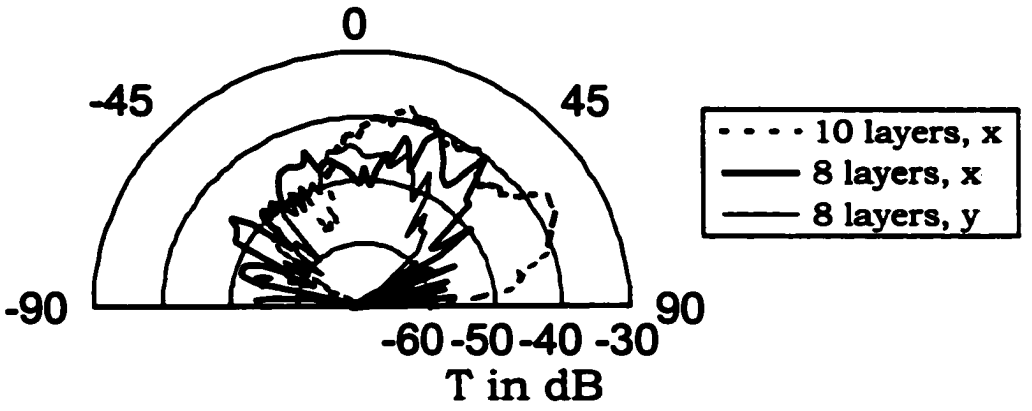


Figure 5.8: Radiation patterns in the x- and y-directions for an 8-layer photonic crystal horn, and in the x-direction only for 10- and 12-layer photonic crystal horns at 11.8 GHz.

for an 8-layer horn and in the x-direction only for 10- and 12-layer horns. All of the radiation patterns measured were relatively broad. We observed a dip in the main lobe for 8- and 10-layer horns that disappeared for the taller 12-layer horn.

Up to this point we have studied horns with a symmetrical opening angle of 40 degrees. At this opening angle we cut one additional rod per two layers of distance measured from the horn's vertex. The resulting horn had one rod cut in the first layer, two rods cut in the third layer, three in the fifth layer, and so on. Reducing or increasing this opening angle reduced the amplitude of the signal transmitted in the z-direction. This was presumably due to interference at the horn's side walls. Similarly asymmetrical designs could be used to point the main lobe in other directions. But once again, interference reduced the amplitude of the signal observed at the peak of the main lobe.

As a proof of concept, we built a simple circuit that consisted of two horns linked by a waveguide. To avoid recording signals reflecting off the

surface of the crystal we placed the two horns on opposite sides of the crystal. The transmission spectrum is shown in Figure 5.9. Note that our measurement recorded transmission for frequencies outside the photonic bandgap of the crystal. Waves at these frequencies could propagate from the transmitting horn to the receiving horn in a straight line since the bulk of the crystal was transparent.

To conclude, we have successfully constructed and characterized a horn antenna integrated into the surface of a photonic bandgap crystal. We examined transmission as a function of horn size, horn style, and frequency. Additionally we examined the radiation pattern as a function of horn size and opening angle. Finally we have successfully demonstrated the use of horns for coupling into photonic crystal

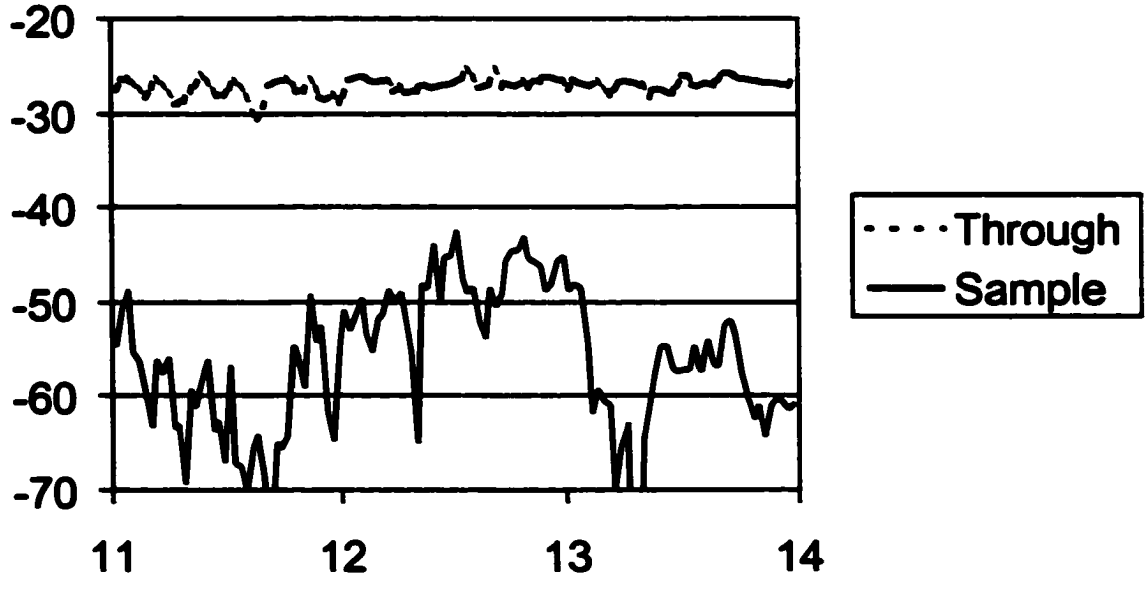


Figure 5.9: Transmission spectrum for a simple photonic waveguide circuit consisting of a waveguide segment and two photonic crystal horns. The spectrum was measured using metal horns placed 25 cm each from the openings. "Through" denotes a second spectrum, recorded for the metal horns, 50 cm apart.

**waveguides by building a simple circuit consisting of a pair of horns connected by a waveguide. The horns studied here should be suitable for optical wavelengths.**

# CHAPTER 6. PBG WAVEGUIDE BENDS

## General Considerations

Four different types of waveguides embedded in a 3-D layer-by-layer photonic bandgap crystal were joined in pairs, forming 90-degree bends. The frequency responses of the resulting waveguide bends were measured and compared to the frequency responses of the individual waveguides.

Tightly confined waveguides can be constructed in photonic bandgap crystals by removing material along the waveguide's axis. The frequency response is a function not only of the photonic bandgap crystal used, but also of the placement and direction of the waveguide. Waveguides running in mutually orthogonal directions can be used to form a three-dimensional network. Waveguides running in the x- and y-directions can be of the same design, since the periodicity of the crystal is the same in those two directions. The periodicity of the photonic crystal differs in the *z*-direction from the x- and y-directions, forcing one to use a different waveguide design for this direction. When constructing a three-dimensional network it becomes necessary to consider coupling between the different waveguide types.

Each waveguide type has a unique frequency response and mode structure. While the frequency response of individual waveguides has been recorded in the past, there is little information on coupling between different waveguide types, which, as mentioned above, is a prerequisite to being able to construct three-dimensional networks. Even if the frequency response of two connected waveguides overlap, the mode structure may

not, making the resulting frequency response more complex than either one of the individual frequency responses.

The waveguides discussed here were all embedded in a layer-by-layer dielectric photonic bandgap crystal. The crystal used (Figure 6.1) was constructed from square alumina rods, 3.2-mm wide with a measured index of refraction of 3.0. Rods were placed in layers with a center-to-center spacing of 1.1 cm, giving a fill factor of 29%. The crystal was 12 layers thick, with a measured photonic bandgap from 11.2 to 13.3 GHz along the rods and from 10.4 to 15.7 GHz along the substrate normal. An attenuation of 21 dB per unit cell at midgap has been reported.[16]

Waveguides were constructed within the crystal by removing rod fragments, or entire rods, forming a hollow area around the waveguide axis. In this paper Li's[21] waveguide names are used, in particular Type X, Type II Y and Type II Z. In addition Type II Z-2 is defined. The letter in the waveguide's name denotes the direction in which the waveguide

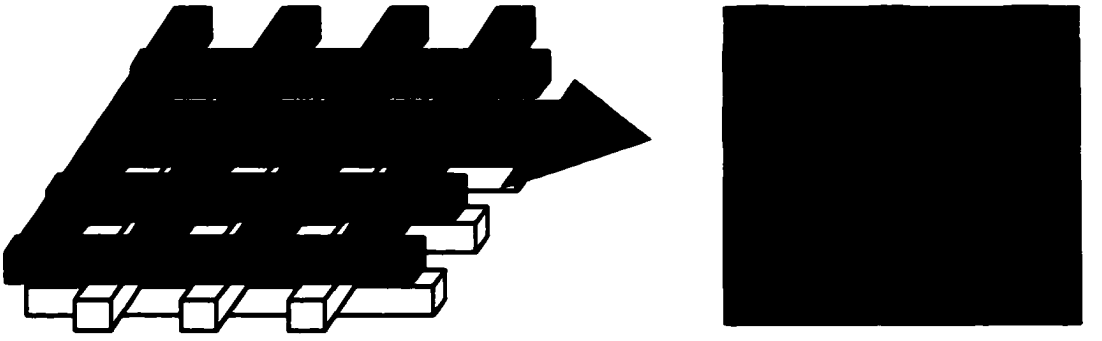

Figure 6.1: Diagram and photograph of a Type X waveguide embedded in a layer-by-layer photonic bandgap crystal. The diagram shows a four-layer crystal with the embedded waveguide. The picture shows a view of the waveguide opening in the crystal surface.

prototype runs, if located in the first layer of the crystal. The Roman numeral "II" in the waveguide's name refers to the symmetry of the wavguide's cross section. Type II waveguides have an asymmetrical cross section; symmetrical Type I waveguides are not discussed here. The Arabic number 2 in Type II Z-2 refers to the fact that this waveguide was constructed by removing two rod fragments per lattice constant.

Type X waveguides (Figure 6.1) were constructed by removing a single rod from the crystal, along the waveguide's axis. Type Y waveguides (Figure 6.2) were more involved in their construction. The waveguide's

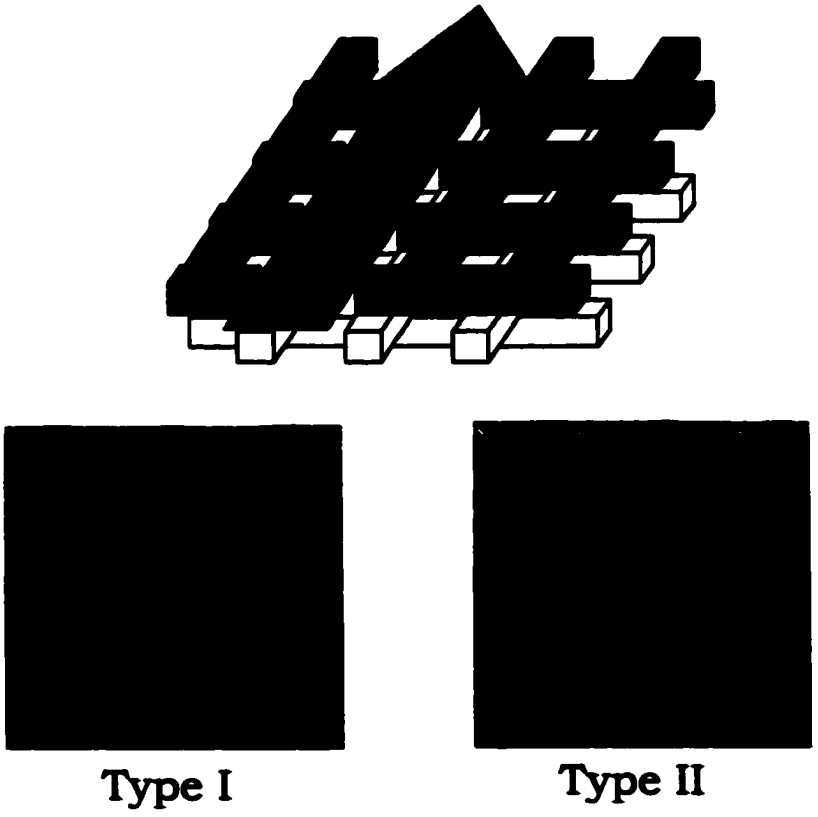


**Figure 6.2: Diagram and photographs of Type Y waveguides. The diagram on the top shows a four-layer crystal with the embedded waveguide. The pictures at the bottom show Type I Y and Type II Y waveguides. These waveguides differ in symmetry.**

axis was located in a layer where it ran perpendicular to the rods of that layer. Rod fragments centered on the waveguide axis were removed. To form a Type II waveguide, the waveguide axis was centered in the gap between the closest rods in the layers above and below the waveguide.

Finally, Type II Z waveguides (Figure 6.3) were constructed by removing rod fragments along a waveguide axis running in the z-direction. The axis of the waveguide was placed in such a fashion that it intersected only one rod per lattice constant. A waveguide of Type II Z-2 was constructed by removing two rod fragments per lattice constant.

**Frequency Response**

A HP 8510 network analyzer was used to record the frequency response of the waveguides and 90-degree bends. The frequency response was measured from 10 to 15 GHz (Figure 6.4). This frequency range covered the entire photonic bandgap of the crystal, as well as frequencies

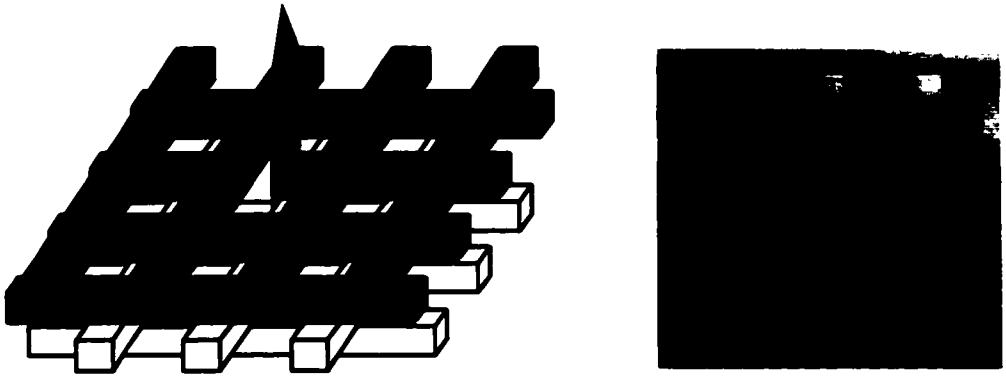

Figure 6.3: Diagram and photograph of a Type Z waveguide embedded in a layer-by-layer photonic bandgap crystal. The diagram shows a four-layer crystal with the embedded waveguide. The picture shows a view of the waveguide opening in the top surface of the crystal.

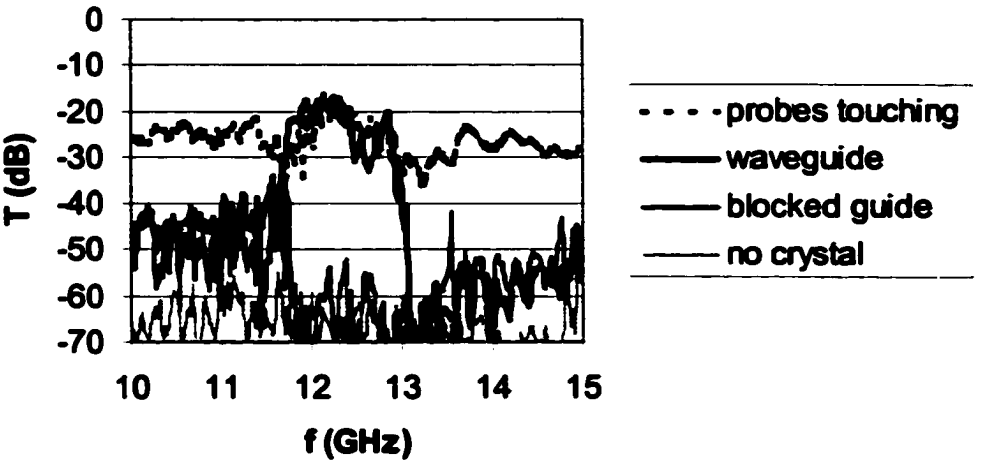


Figure 6.4: Frequency response graph of a Type X waveguide

close to the bandgap edges. Coupling probes inserted into the waveguide openings were used to excite the waveguide. These probes were connected to the network analyzer with coaxial cables. The probe's design was selected for the broadest frequency response and flatness, not maximum gain. The probes were carefully placed in the waveguide openings because the placement of the probes affects coupling efficiency. For single-mode waveguides the probes were placed for maximum coupling while maintaining a flat frequency response.

Four frequency response measurements are presented in Figure 6.4. The first trace was measured with the coupling probes touching each other inside the waveguide. This measurement allowed one to estimate coupling loss, which was seen to be on the order of 14 dB per probe. One could use this knowledge to normalize the remaining measurements presented in Figure 6.4. We were reluctant to perform such a normalization since it would be valid only for Type X waveguides. Measurements with other waveguide types would have to be normalized

separately, with measurements containing more than one waveguide type requiring a separate solution.

The remaining two measurements in Figure 6.4 were taken with the waveguide blocked and with the crystal removed. These measurements were taken to verify that surface or other leakage modes did not influence the measurement results. We observed that due to the high attenuation of the bulk crystal, evanescent waves traveling parallel to the waveguide axis outside the waveguide should have little effect on the frequency responses measured.

Some waveguides studied had multiple modes. Modes that did not overlap in frequency could be observed as separate bands in the transmission spectrum. In such cases the coupling probes were positioned so as to excite the largest number of modes possible. Other than adjusting the coupling probes, the waveguides and 90-degree bends were measured "as built." It would be possible to modify the frequency response of the waveguide bends by including tuning stubs or cavities, but this was not done here.

First, the frequency response of straight waveguide segments was recorded (Figure 6.4). The Type X waveguide had the greatest bandwidth of the waveguides presented. A single waveguide mode seemed to be responsible for the bulk of the transmission frequency range, leading to a relatively flat frequency response.

A more concise graphical representation of frequency response is presented in Figures 6.5, 6.9, and 6.10. Portions of less than 10 dB loss in relation to the transmission maximum are shown as black bars. Peak

transmission values were found at -14 to -20 dB. Considering a coupling loss of 14dB this suggests low loss transmission. The numbers used were rounded to the nearest 0.025 GHz. The frequency responses of multiple waveguide configurations are shown on the same frequency scale, with individual responses labeled along the right of the diagram. This allows the display and comparison of a large number of different waveguide bends.

The response of the Type II Y waveguide (Figure 6.5, line 2) may include multiple waveguide modes. Two transmission regions could be noticed, one from 11.8 to 12.1 GHz and a second region extending from 12.2 to 12.8 GHz. Moving the coupling probe enhanced the higher-frequency region while attenuating lower frequencies, further suggesting the presence of two modes with spatially distinct nodes.

Two waveguide types running in the *z*-direction were studied. Both displayed multiple transmission modes. Type II Z had a frequency


**Figure 6.5: Frequency response of Type X and Type II Y waveguides and bends.**

response with several narrow transmission regions, with the widest one extending from 12.2 to 12.4 GHz. The major region for the Type II Z-2 waveguide extended from 12.5 to 12.8 GHz.

Two of the four waveguide types discussed can be connected to a second waveguide of the same type to form a 90-degree bend. This was possible for Type X and Type II Y, by placing the two waveguides in neighboring layers, as shown in Figure 6.6. There was a total of three such 90-degree bends, two of which were for the asymmetrical Type II Y waveguide. Type Z waveguides ran in the z-direction, and thus could not be connected to a waveguide of the same type, since any connecting waveguide layed in the x-y plane.

Looking at the frequency response for the Type X bend (Figure 6.5), it can be seen that the bend favored the lower frequency transmission mode. A second mode from 12.7 to 12.9 GHz was present, but highly attenuated. The Type X bend measurements were in general agreement with M. Bayindir et al.[7] The transmission dip at 12.2 GHz observed by Bayindir was absent in the measurements presented here, probably because a different coupling method was used.

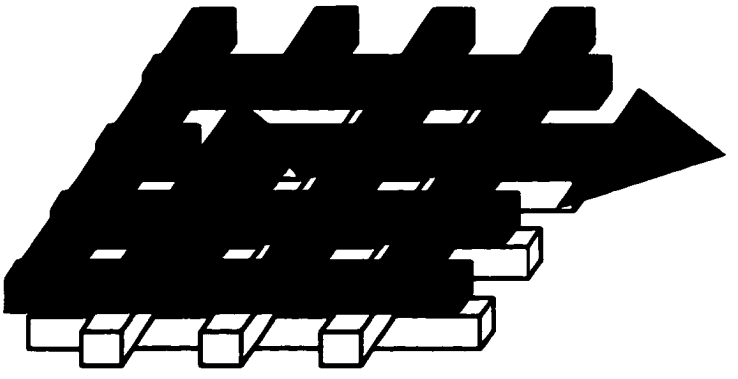

Figure 6.6: Diagram of a Type X waveguide bend embedded into two layers of a photonic bandgap crystal.

There were two possible bends for the Type II Y waveguide, due to the waveguide's asymmetry. A "symmetrical" bend could be constructed, where the same side of the waveguide would remain pointed to the inside of the bend. An "asymmetrical" bend was formed when the waveguide was flipped within the bend. The side of the waveguide that pointed to the inside of the waveguide before the bend pointed to the outside of the bend after the bend. Examining the frequency response of the bends (Figure 6.5), it could be seen that both Type II Y bends transmitted large portions of the Type II Y frequency spectrum. The frequency responses differed in that the asymmetrical bend transmitted frequencies from 12.1 to 12.4 GHz better than the symmetrical bend.

A Type X waveguide could form a bend with a Type II Y waveguide with both waveguides contained in the same layer of the crystal (Figure 6.7). Unlike the other intersections presented here, only a single layer of crystal needed to be modified during construction. The possibility of constructing such a waveguide bend was mentioned by Chutinan and Noda, but not further examined by them.[6] Good coupling was observed

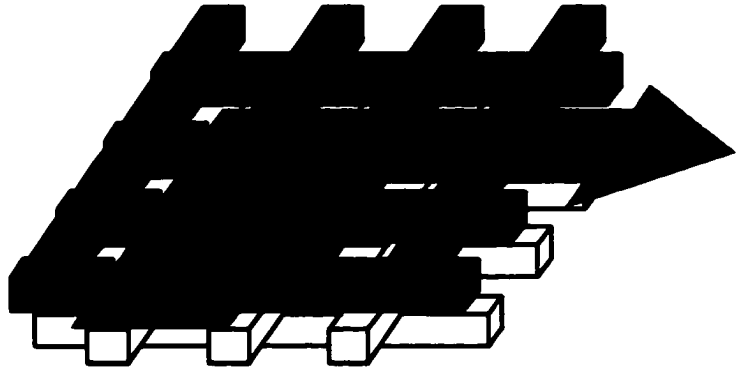

Figure 6.7: Diagram of a Type Y waveguide connected to a Type X waveguide. This connection forms a bend that can be embedded into a single layer of a photonic bandgap crystal.

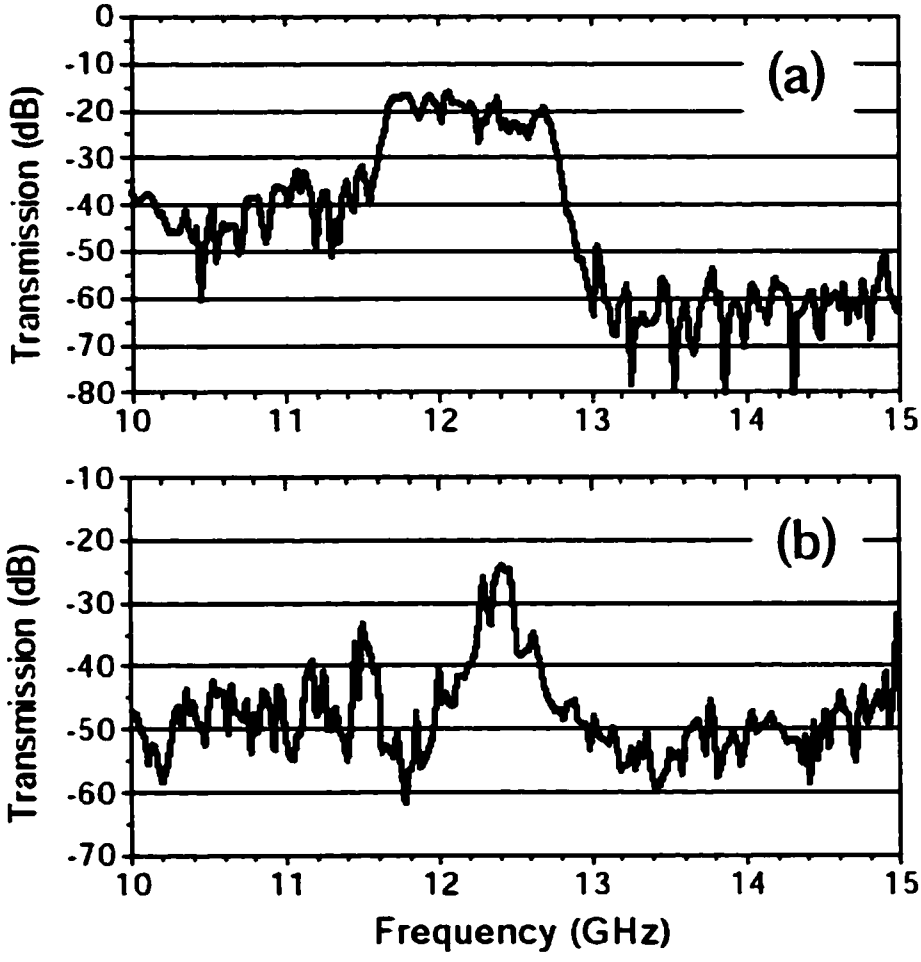


**Figure 6.8: Transmission spectra for wave propagation through waveguide bends: (a) Type X waveguide connected to a Type II Y. This bend can be built into a single layer of the photonic crystal. (b) Type X connected to a Type II Z.**

for this waveguide bend (Figure 6.8). The frequency pass band of this bend (Figure 6.5) extended from 11.6 to 12.9 GHz.

A large number of distinct 90-degree bends could be formed between the two Type Z waveguides and waveguides in the x-y plane. The Type II Z waveguide could be connected to the waveguide in the x-y plane in two possible orientations (Figure 6.3). It could be oriented to make the missing rod segments in the Type II Z parallel to the axis of the waveguide

in the x-y plane. The rod segments removed to form the Type II Z waveguide and the axis of the other waveguide now lie in the same plane. The other possible orientation rotated the Type II Z waveguide by 90 degrees around its axis, making the Type II Z waveguide's missing rod segments perpendicular to the plane formed by the axis of the two waveguides. Graphs of the frequency response of all eight possible waveguide intersections are presented in figures 6.9 and 6.10, but are not discussed individually.

Several observations can be made when looking at the frequency responses presented. First and foremost, all of the bends studied passed at least one frequency. Frequencies that lie toward the center of the modes of both waveguides forming the junctions seemed to couple best. Conversely, attenuation increased toward the edges of the transmission frequency regions. Often the frequency response of the waveguide bend differed from the product of the frequency responses of the individual

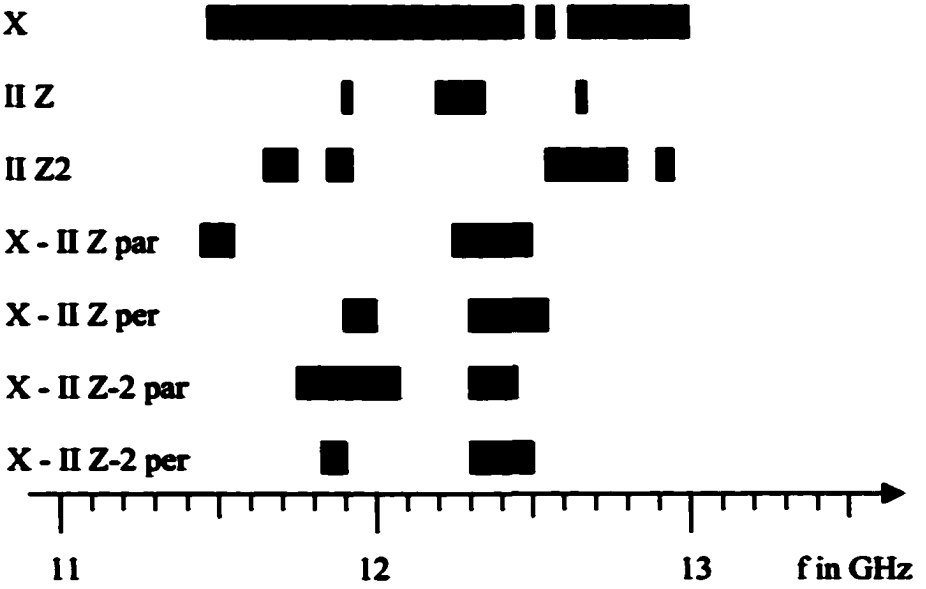


Figure 6.9: Frequency response of Type X and Type II Z waveguides and bends.

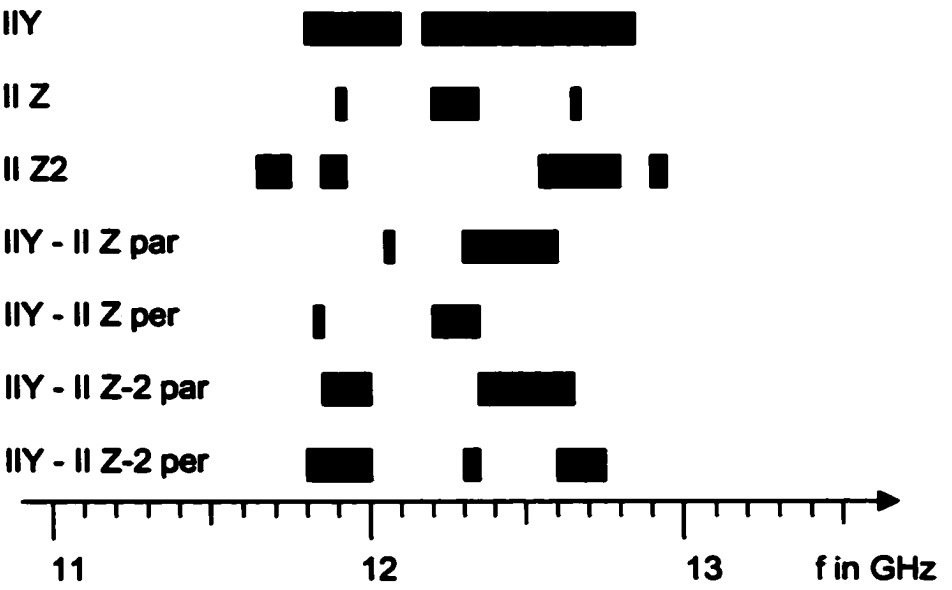


Figure 6.10: Frequency response of Type IIY and Type II Z waveguides and bends.

waveguide sections. Waveguide modes observed in both straight segments were sometimes suppressed by the waveguide bends. This may have been due to insufficient spatial overlap of the modes of the two segments.

In a few cases, waveguide modes that were difficult to observe in straight waveguide segments were observed in the waveguides forming a junction. One possible explanation is that the waveguide bend was able to couple to modes, which were not excited by the coupling probes in a straight waveguide segment, due to the positioning of the coupling probes. A second, but less likely, explanation is that non-propagating modes were detected by the coupling probes. This is unlikely due to the distance between the vertex of the bend and the coupling probes. One is left with the first explanation: Not all of the propagating modes were excited in the measurements of the straight waveguide segments.

Examining the observed frequency responses, one can conclude that all of the bends possible among the four waveguide types studied pass at least one frequency band. One can use a combination of waveguides to connect any pair of locations within the crystal. Suitable waveguides can be chosen by referring to Figures 6.5, 6.9, and 6.10. The measured pass bands of the different bends overlap sufficiently to allow for the construction of waveguide networks using a combination of Type X, Type II Y, and Type II Z segments.

# CHAPTER 7. PBG WAVEGUIDE TRANSMISSION LOSS

There are three possible loss mechanism for waves propagating in a photonic crystal waveguide: leakage to the surface of the crystal; dissipation in the materials used; and reflections at discontinuities, such as bends or imperfections. Dissipative losses play only a minor role in the waveguides studied here, but they determine the value of the lowest possible loss. Losses due to reflections affect complex waveguide structures, such as bends, but play only a minor role in straight waveguide segments.

Loss is primarily caused by waves leaking from the waveguide to the surface of the crystal. For the crystals used here this could be the top surface parallel to the substrate, or one of the sides perpendicular to the substrate. The top was the largest surface. While it was easy to move a waveguide away from the side of the crystal, it would always be close to the top. Thus leakage to the top (and bottom) warranted careful examination. This will be discussed later in the chapter.

## Edge Loss

Loss out of the sides of the crystal is less important but should nevertheless be examined briefly. To avoid waveguide losses due to evanescent waves leaking through the bulk crystal to the waveguide surface, the waveguide has to be embedded in the bulk of the crystal, away from the top and side surfaces. To determine the minimum distance needed between the waveguide and the sides of the crystal, it is useful to look at waveguide loss as a function of distance to that edge. Examining

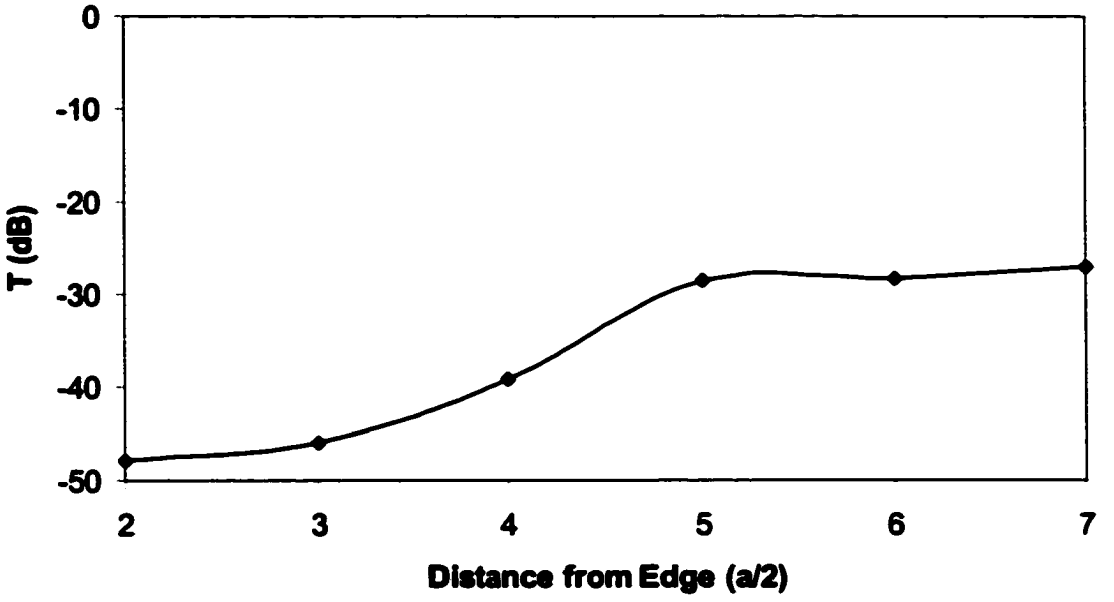


Figure 7.1: Graph of loss as a function of distance from edge for Type X waveguides.

Figure 7.1, it can be seen that transmission loss decreased as the distance to the edge was increased; it reached a plateau once the distance to the edge was greater than 2.5 lattice constants. Similar observations were made if the waveguide was moved in the *z*-direction. This agrees with theoretical calculations.[6] For the remaining measurements waveguides are located three or more lattice constants from the edges of the crystal, unless specifically stated.

**Surface Loss**

A 12-GHz waveguide was constructed within a centimeter-scale three-dimensional photonic crystal made from stacked-layers of alumina rods by removing one rod. The loss in this waveguide was measured as a function of length and distance from the waveguide's axis to the nearest

edge of the crystal. The empirical function describing this loss was found. It is useful for determining the minimum amount of crystal needed to surround a waveguide for an acceptable loss value. Thus crystals could be tailored for an application's acceptable loss, allowing one to use the minimum amount of material necessary.

This section presents a measurement of loss for a waveguide embedded in a 3-D photonic crystal. For waveguides in sufficiently thin photonic crystal slabs, propagation loss is primarily caused by the proximity of the crystal's edge. Little quantitative loss data has been presented in the past.[7] We examine waveguide loss as a function of length and of the distance to the surface of the crystal. The loss measured is comparable to the losses reported recently for photonic bandgap waveguides in 2-D materials.[22,23]

The two predominant types of photonic crystal waveguides are waveguides embedded in three-dimensional photonic crystals and waveguides embedded in two-dimensional photonic crystals, with the index of refraction guiding making up for the third dimension. Waveguides embedded in 2-D materials have the advantage of being easy to fabricate, but they are difficult to make low-loss. This is because bends in two-dimensional waveguides cause mode conversion into leaky modes, which subsequently dissipate.

The loss measurement presented here was performed on Type X waveguides embedded zero to eight layers into the crystal. While one particular waveguide is presented, the same measurements have been carried out for other waveguide types, yielding similar results. This

measurement technique can thereby be used for comparing the loss of different waveguide types, independent of coupling loss.

Removing a single rod from this photonic crystal opened a highly confined waveguide[5,6] running the length of the crystal for frequencies from 11.5 to 12.6 GHz, with openings at two opposite crystal faces. Electro-magnetic radiation could be coupled into one end and follows the waveguide to the other end where it could be coupled out.

Coupling probes connected the waveguide to a HP 8510 network analyzer. These coupling probes had a flat frequency response rather than a low loss. The effective waveguide length was determined by how far the coupling probes were inserted. We used a fixed frequency of 12 GHz, close to the center of the waveguide's pass band, for the remaining measurements.

Individual losses added up to a system loss on the order of 30 dB for a short waveguide and its coupling probes. The bulk of this was coupling loss. Coupling loss was independent of length, but dissipative loss (in dB) was a linear function of length. Dissipative loss within the waveguide is expected to be low. Loss due to evanescent waves originating at the waveguide and leaking out of the crystal made up the balance. This loss (in dB) was a linear function of waveguide length, but we also expected to see a loss component following a negative exponential function of the distance to the nearest crystal surface. This was due to evanescent waves leaking to the surface. They decayed exponentially in field strength as a function of distance. Thus these individual losses

could be measured indirectly by varying the waveguide's length and the distance to the nearest crystal surface.

We measured transmission as a function of waveguide length by first inserting one coupling probe far enough into the waveguide to touch the other probe, then slowly withdrawing it while recording the transmitted amplitude as a function of length (Figure 7.2). This measurement allowed us to find propagation loss independent of coupling loss. Next, the distance from the waveguide axis to the surface of the crystal was varied from zero to eight layers in nine steps by removing layers of rods from the crystal's surface, and additional propagation loss measurements were taken by repeating the measurement sequence described above (Figure 7.3). These additional measurements allowed us to examine the loss due to evanescent waves leaking to the crystal's edge.

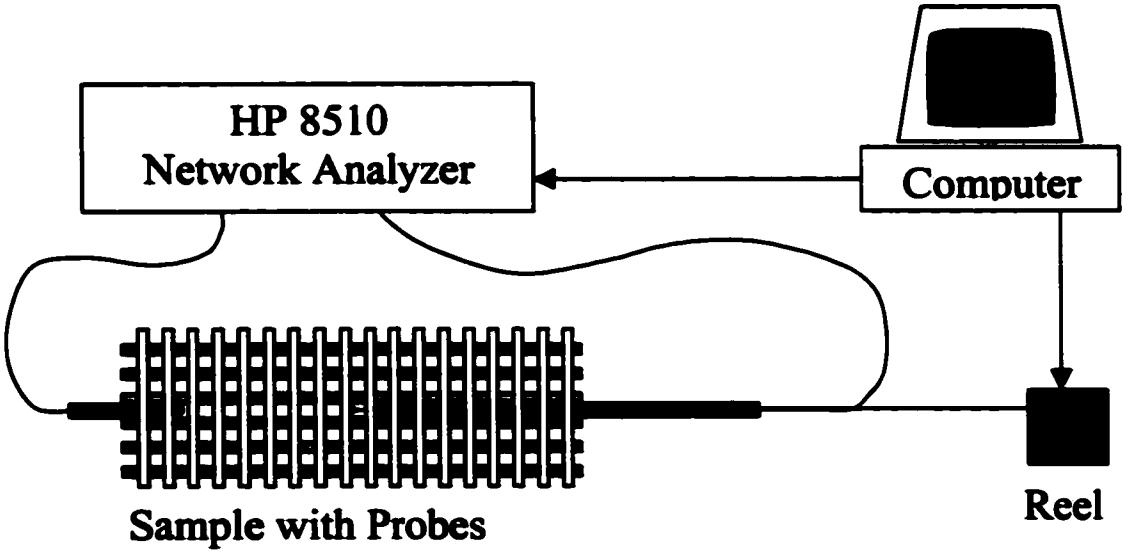


Figure 7.2: Loss is measured as a function of length by moving one of the coupling probes. A computer controls the motion of the probe and records the data.

We first analyzed the data for the individual loss measurements. Each series contained loss as a function of length for a particular waveguide configuration. The slope of a linear curve fit revealed the loss per lattice constant, and the offset revealed the loss due to coupling, as shown in Figure 7.4. This allowed us to separate coupling loss from propagation loss. We plotted the waveguide loss figures for all the waveguide measurements into a common graph as a function of distance between the waveguide axis and the nearest surface (Figure 7.5). Because this figure shows loss due to evanescent wave leakage, it could be fit appropriately using an exponential curve.[24] This curve allowed us to estimate loss for a distance from the waveguide to the crystal surface. We could use this fit as a starting point for setting up measurements with longer waveguides, or experiments at shorter wavelengths. The measured

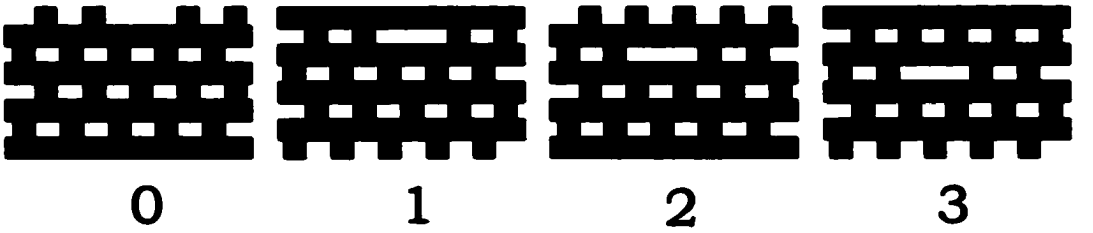


Figure 7.3: Loss is also measured as a function of the number of layers between the waveguide and the surface.

loss could also be used to compare different waveguides independent of coupling loss.

Not surprisingly, the lowest loss was observed for a waveguide embedded deep into the crystal, with a distance of two lattice constants to the crystal surface. The average loss observed for this waveguide was

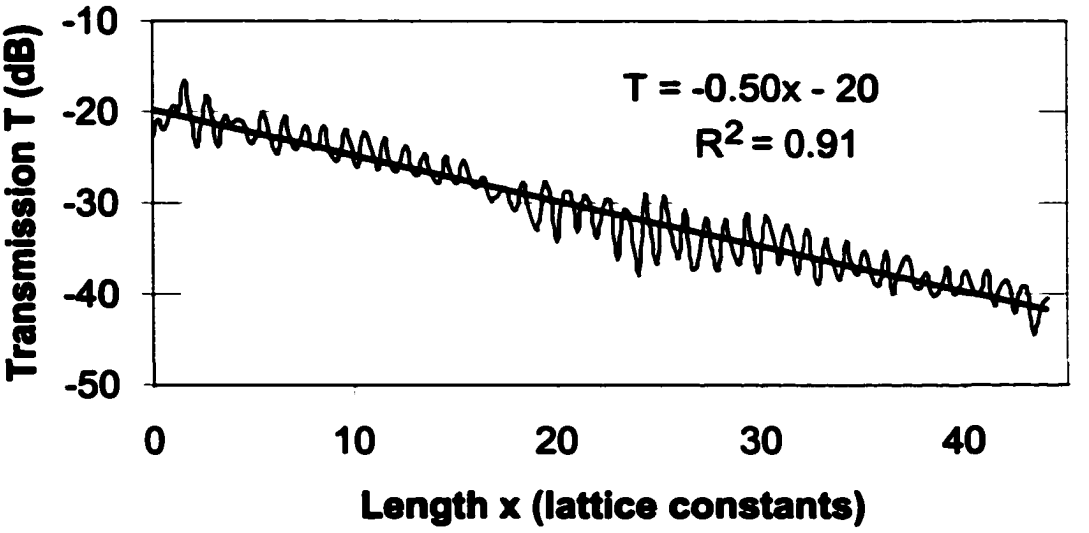


Figure 7.4: Loss as a function of waveguide length. The oscillations are due to the probe coming into close proximity with individual rods. The guide examined has two layers of cladding.

0.028 dB per lattice constant, which converts to 0.063 dB per free-space wavelength.

It is of interest to compare the above losses to the loss figures reported for two-dimensional photonic crystal waveguide structures. The lowest losses reported for photonic waveguides were measured in structures designed for infrared wavelengths. For straight two-dimensional photonic crystal-based waveguides, a loss of 0.017 dB per free-space wavelength at 1500 nm has been reported for a silicon air bridge,[22] and 0.021 dB per free-space wavelength at 1040 nm for a GaAs waveguide with Ga(Al)As cladding on a GaAs substrate.[23]

Our measurements predict that to obtain comparable loss 2.5 lattice constants of cladding are required. For 2.5 lattice constants the loss extrapolates to 0.014 dB per free-space wavelength. With data covering 0 to 2 lattice constants, 2.5 lattice constants is still a reasonable

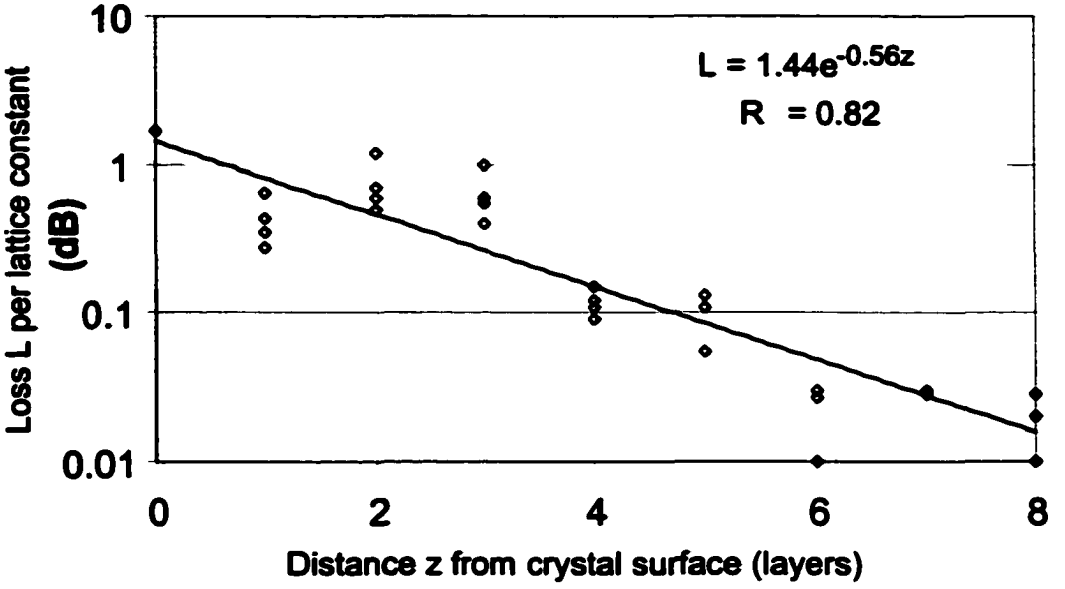


Figure 7.5: Loss per lattice constant as a function of the distance from the waveguide axis to the crystal's surface.

extrapolation. Obviously the extrapolation needs to be handled carefully since for a large number of cladding layers dissipative losses, which are not considered here, will begin to contribute to the total loss.

We have demonstrated a new measurement technique for measuring losses in photonic crystal waveguides and have used this technique to measure the loss for a three-dimensional photonic crystal waveguide, thus providing an upper boundary for its loss. By extrapolating our data we were able to determine the cladding thickness our three-dimensional crystal waveguide requires to achieve losses comparable to the lowest losses reported for two-dimensional crystal-based waveguides.

# CHAPTER 8: PBG WAVEGUIDE DISPERSION

We have mapped dispersion for a 12-GHz waveguide segment contained within a centimeter-scale three-dimensional photonic crystal. We performed reflection and transmission measurements on this waveguide segment, recording the signal as a function of frequency and length, and found the dispersion spectrum by performing a discrete spatial Fourier transform. The measured mode structure was compared to a mode structure calculated using a plane-wave expansion method combined with a supercell technique. We found that our measurement and analysis technique produced modes that agreed with the general shape of the theoretically calculated modes.

We were interested in mapping out the dispersion relation for the propagating modes. The dispersion relation characterizes the speed of wave propagation as a function of frequency. Li and Ho[21] have developed a method to calculate band diagrams for three-dimensional photonic crystal waveguides. We will compare our measurements to this theory and see how well they agree.

## Prior Work

Traditionally the propagation wavelength has been measured using a slotted line measurement.[25] In this measurement a probe was used to map the amplitude of a standing wave inside a waveguide segment of interest, which was mismatched at its termination to produce the standing wave. For single-mode waveguides the propagation wavelength was two times the distance between a pair of successive peaks.

Bayindir et al. presented a dispersion diagram, that displayed only one propagation mode for the waveguide studied.[7] They examined phase and amplitude as a function of frequency for a fixed waveguide length, and extracted the wave vector $k$ by analyzing the phase shift in comparison to free space. Their analysis assumed a single-mode waveguide.

Loncar et al.[26] mapped the dispersion for leaky waves in a two-dimensional photonic crystal waveguide. Loncar used a Fourier transform to examine the amplitudes of a leaky standing wave for spatial periodicity. They did not measure phase. Their analysis generated a graphical representation of the dispersion spectrum.

It is interesting to note that a photonic crystal waveguide cannot be single-mode. This is due to the periodic nature of the crystal, which provides us with Brillouin zones, with each mode existing in each Brillouin zone. This does not necessitate wavelength dispersion. All copies of a particular mode have the same slope, and thus the same group velocity, meaning that the energy propagates at the same speed, regardless of the Brillouin zone in which it propagates. Due to the crystal's periodic nature we can no longer assume a single-mode waveguide. We need to use a measurement and analysis method suitable for multimode waveguides.

**Theory**

We started our experiment by measuring the frequency and phase response of a waveguide along its axis as a function of length in the x-

direction. This measurement captured information about a wave with wavenumber $k_n$. Assuming a waveguide-like solution, we can express the electric field $\vec{E}$ in the waveguide as $\vec{E} = \sum_n \vec{A}_n(y,z,\omega)e^{ik_n x - i\omega t}$, where $\vec{A}_n(y,z,\omega)$ contains the spatial shape of the $n$th propagating mode for a particular frequency ω. We use a probe with response $\vec{P}(x,y,z,\omega)$ to sample the signal at the end of the waveguide. This produces an electrical signal $T(x) = \sum_n \left[\vec{P}(x,y,z,\omega) \otimes_{x,y,z} \vec{A}_n(y,z,\omega)e^{ik_n x - i\omega t_0}\right|_{y,z=0}$. We use $\otimes_{x,y,z}$ to denote the dot product convolution in respect to x,y,z.

We combine $\vec{A}_n(y,z,\omega)$ and $\vec{P}(x,y,z,\omega)$ into $B_n(x,\omega)$, such that $B_n(x,\omega) \equiv \left[\vec{P}(x,y,z,\omega) \otimes_{y,z} \vec{A}_n(y,z,\omega)\right|_{y,z=0}$. Thus, $T(x) = \sum_n B_n(x,\omega) \otimes_x e^{ik_n x - i\omega t_0}$. The Fourier transform is $T(k) = e^{-i\omega t_0} \sum_n B_n(k,\omega)\delta(k_n - k)$ with $\delta$ denoting the Dirac delta. The phase offset $e^{-i\omega t_0}$ can be discarded by taking the absolute value of $T(k)$.

If we measure $T(x)$, a plot of the Fourier transform $|T(k)|$ will show lines for all the modes $k_n$. The effect of the detector response $P(x,y,z,\omega)$ is to modulate the amplitude of the lines. The broadening of the lines is due to the finite size of the data set in the spatial x-direction. Thus we can use a Fourier transform to map the dispersion function given the data from the spatial domain.

**Experiment and Analysis**

The photonic bandgap crystal used here was constructed in a layer-by-layer fashion.[16] We used square alumina rods of 3.2-mm width and with a measured index of refraction of 3.0. This photonic crystal has a filling ratio of approximately 29%, and a three-dimensional photonic

bandgap extending from 11.2 to 13.3 GHz. Our crystal was 4.5 lattice constants thick (that is, 18 layers), 14 lattice constants wide, and 56 lattice constants long (6.4 cm * 15.2 cm * 61 cm long).

Removing a single rod from this photonic crystal opened a highly confined waveguide[5,6] running the length of the crystal for frequencies from 11.5 to 13.1 GHz, with openings at two opposite crystal faces. For this experiment a stationary coupling probe was inserted into one opening, and a movable coupling probe in the other. The distance between the tips of the two coupling probes determined the effective waveguide length through which the signal propagated.

The coupling probes connected the waveguide to coaxial cables hooked to a HP 8510 network analyzer. The probes had a flat frequency response rather than a low-loss. EM radiation was coupled into one end of the waveguide and followed it to the other end where it was detected. The amplitude and phase of the detected signal were recorded by the network analyzer.

We measured transmission and reflection as a function of waveguide length by first inserting the movable rod far into the crystal, thus reducing the waveguide length to 7 cm. The network analyzer recorded the signals as a function of frequency from 11 to 13 GHz. Next the probe was moved under computer control and the spectrum measurement was repeated for a total of 320 evenly spaced waveguide lengths.

For each frequency, we used a spatial discrete Fourier transform to calculate $T(f,k)$, giving us amplitude as a function of wave number and

frequency. This was the dispersion relation spectrum for our waveguide, which we plotted in Figure 8.1. Note that the axes were frequency f and wave number $k/2\pi$.

In the dispersion diagram we saw two transmission modes, which were labeled in Figure 8.1b. A higher frequency mode Ia extended from 12.2 to 13.6 GHz, and a second, lower frequency mode Ib and Ic extended from 11.6 to 12.6 GHz. The two modes overlapped in frequency from 12.2 to 13.1 GHz. Both modes a and c displayed regions of constant slope, where dispersion was minimal. Mode segment Ib had a negative slope. The slope of the dispersion curve represents group velocity. We observed positive as well as negative group velocity.

Examining the higher order Brillouin zones, we found repeats of some of the propagation modes, as one would expect. Mode c was the strongest; it was observed in zones I, II, III, IV, and VI. This gave us confidence in our measurement and analysis technique, and in having correctly located the Brillouin zone edges.

The other curves, labeled $\alpha$, $\beta$, $\gamma$ and $\varepsilon$ in Figure 8.1b, could be explained by considering reflection and mode conversion at the probes. For waves that have traveled several times along the waveguide, our data analysis shows an effective $k_e$, which was the sum of the $k$ vectors of the segments and not necessarily a physical mode. In general $k_e = \sum_i k_n$ for a wave that traversed the waveguide three times by being reflected once at each end. The modes $k_m$ and $k_n$ could be positive or negative. Examining artifacts $\alpha$, $\beta$, $\gamma$, and $\varepsilon$, we found that they all fit the form $k_e = 2 * k_m + k_n$.

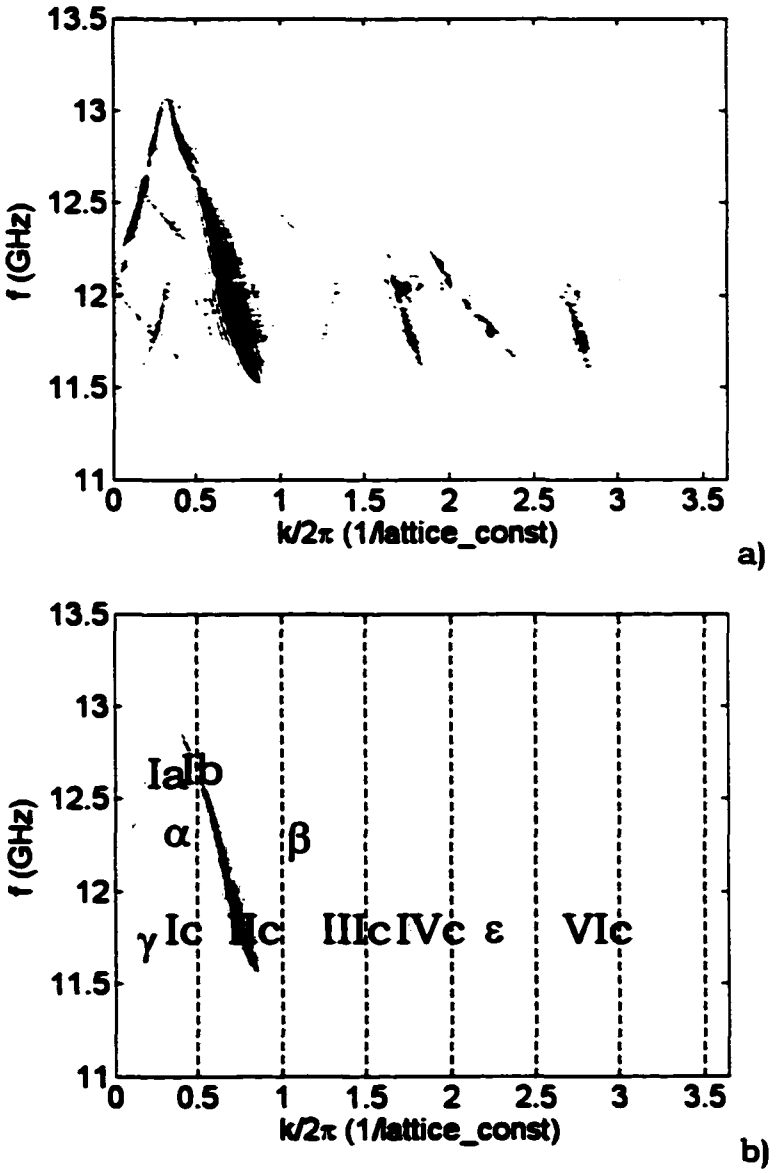


**Figure 8.1: (a) Measured dispersion spectrum; (b) Dispersion spectrum with the individual modes labeled. The Brillouin zone boundaries are indicated by dashed lines.**

In Figure 8.2 we have plotted the measured dispersion spectrum for the first Brillouin zone, as well as a theoretical prediction of the modes for comparison. These curves were calculated using a planewave expansion method combined with a supercell technique.[21] The predicted modes

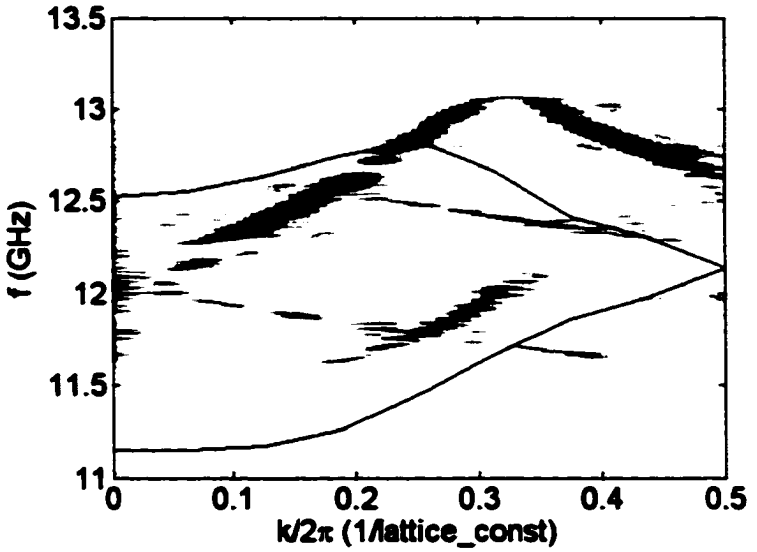


Figure 8.2: First Brillouin zone, with theoretically calculated bands overlaid.

displayed the same characteristic shape as the modes measured, but were shifted in the direction of smaller k as well as lower frequencies.

Using our initial data set, one could also perform time domain reflectometry. To do this the data would be converted from the frequency to the time domain using a Fourier transform. One could examine the arrival times of the signal to detect reflections. This could be used to examine waveguide structures for discontinuities.

In conclusion we developed a method for waveguide dispersion mapping suitable for multimode guides. Using this method, we mapped the dispersion curves for a waveguide embedded in a three-dimensional photonic crystal. We were able to explain all features of our resulting dispersion relation spectrum. The modes recorded clearly illustrate the multimode nature of the waveguide studied. We gained confidence in our method by examining the periodicity across the Brillouin zones, and observing agreement in shape with theoretical calculations.[21] The

knowledge gained improved our understanding of the waveguide presented. Using the experimental method presented, we were able to map the modes for other waveguides (Figure 8.3).

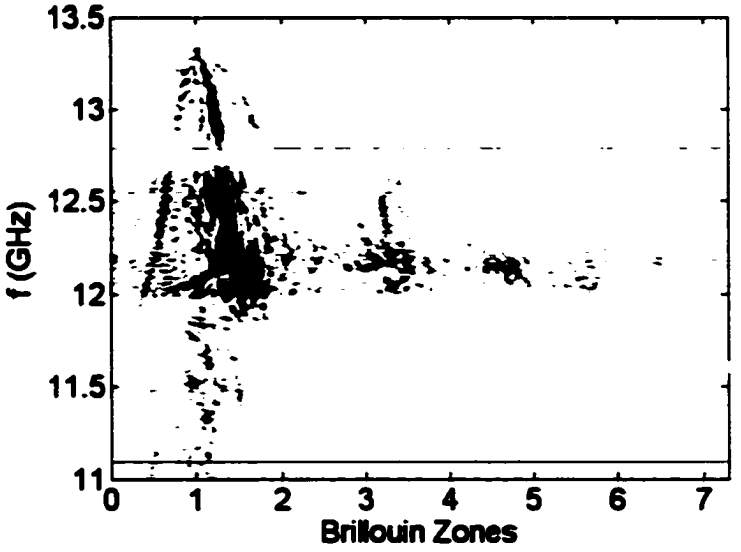


Figure 8.3: Measured dispersion spectrum for a Type II Y waveguide.

# CHAPTER 9. CONCLUSION

In summary, we gained an understanding of the fundamental characteristics of photonic crystal waveguides. After taking a look at traditional waveguides and the history of photonic bandgap crystals, we examined different types of photonic bandgap crystal-based waveguides. We briefly discussed waveguides built in two-dimensional photonic bandgap crystals before moving on to waveguides built in three-dimensional photonic bandgap crystals. We examined the frequency response of several waveguide designs for tightly confined waves.

Our waveguides had to connect to the external world, first for meaningful measurements, then for useful applications. We solved this problem by using coupling probes. Our coupling probes worked best at microwave frequencies. At optical frequencies we expected the losses caused by the metal used in the probes' construction to become prohibitive. This lead us to consider coupling by embedded horns.

After examining coupling we looked at additional waveguide topics: waveguide bends, waveguide transmission loss, and waveguide dispersion spectra and mode mapping. All three are important. They allowed us to move toward a deductive design approach for photonic waveguide circuits, away from the empirical approach used up to this point. Mode mapping allowed us to compare transmission matrix theory to our results. We found agreement in the shape of the modes, but a slight shift in frequency and propagation vector.

All of the photonic waveguide structures presented here were built from a single ceramic dielectric as well as air. This makes the structures

presented fundamentally scalable. We could scale the structures to optical wavelengths and gain knowledge on how to construct useful waveguides once we have the capability to make photonic crystal waveguides at those wavelengths.

Future research opportunities have already been pointed out in the preceding chapters. We focused on waveguides built by removing material; one could examine waveguides built by adding material. Similarly we carried out some of the measurements for the Type X waveguide only. One can examine the other waveguides more thoroughly.

We focused on tightly confined waveguides. One could relax this restriction and examine broader waveguides, maybe even ones that are multiple layers thick. It may be possible to learn more about the underlying guiding mechanisms. One may be able to apply a reflectance plane model similar to Kavanaugh's.[8] One may be able to theoretically derive the parameters used in this model and compare them to experimentally found values.

In this dissertation we examined structures containing only linear materials. Using nonlinear materials and optical pumping one could construct a photonic waveguide-based amplifier.[27] Assume signals $A\cos(\omega t)$ and $B\cos(2\omega t)$ and a photonic crystal with a photonic badgap that includes frequency $\omega$, but not $2\omega$. One could construct a waveguide in this crystal with a guided mode at frequency $\omega$ that would be filled with a nonlinear material. This waveguide could produce amplification. If we applied a signal of frequency $\omega$ and a pump wave of frequency $2\omega$, we could get a new signal within the waveguide $(A\cos(\omega t) + B\cos(2\omega t))^2$ that

produces a signal at $3\omega t$, which dissipates and a signal at $\omega t$ which is guided. This signal has been amplified by a factor of AB.

We see that a wealth of exciting research on photonic crystal waveguides is possible. Photonic crystal waveguide research can be inexpensive. For the research presented we needed access to a network analyzer, which was shared with other projects, a few hundred ceramic rods, and a computer. These materials were not consumed in the course of the research. The main consumable is the readily available superglue used for securing the rods in the crystal. Photonic crystal waveguide research allows one to produce rewarding results on a budget.

We could look even further into the future of photonic bandgap crystal-based waveguides, which takes us to shorter wavelengths. More work and opportunities lie ahead once we leave the microwave domain. The main applications in the microwave regime are antennas and antenna feeds for radar and communication systems. At far-infrared wavelengths other imaging applications besides radar become interesting. Once we venture forth into near infrared wavelengths we encounter fiber optic applications and optical computing, as well as local optical interconnects for semiconductor-based computing.

# APPENDIX: EXPERIMENTAL PROCEDURE

## Construction of K-Band PBG Crystals

The stacked-layer photonic bandgap crystals are assembled as follows. Pairs of layers of rods are glued into sheets, with two layers of rods forming one sheet. Stacking two of these sheets produces a photonic crystal with a height of one lattice constant. The sheets are placed such that the rods in the second sheet are aligned with the gaps in the first sheet. This gives the correct stacking sequence. One can continue stacking layers until the desired thickness is reached. We found it helpful to use the wooden handles of cotton swabs to keep the layers aligned. To do this we carefully threaded the wood through a line of voids in all the layers.

Making sheets of rods requires careful alignment. We used rolled pins that were secured in a sheet of "countertop" material (the compressed wood product used for kitchen counters). It is cheap, easy to clean, and easy to drill. Table A.1 lists the pin spacing used, and Figure A.1 shows the finished alignment jig.

## Experimental Setup

Measurements presented in this dissertation were taken using a HP 8510 network analyzer. An Apple Power Macintosh 7100/80 was used for recording data, and for controlling a Klinger gear motor connected by a Newport MM1000 DC motor controller/driver. A Narda 639 standard gain horn mounted to the gear motor was used for radiation pattern measurements.

Table A.1: Assembly jig pin spacing in standard units. The spacing repeats after 3 inches. Remember to keep the row of pins from interfering with the rods.

| Width of rod or gap | Distance to edge | Distance to center of pin |
|---|---|---|
| 0 | 0 | No pin |
| 0.259 | 0.259 | 0.224 |
| 0.125 | 0.384 | 0.419 |
| 0.304 | 0.687 | 0.652 |
| 0.125 | 0.812 | 0.847 |
| 0.304 | 1.116 | 1.081 |
| 0.125 | 1.241 | 1.276 |
| 0.304 | 1.545 | 1.510 |
| 0.125 | 1.670 | 1.705 |
| 0.304 | 1.973 | 1.938 |
| 0.125 | 2.098 | 2.133 |
| 0.304 | 2.402 | 2.367 |
| 0.125 | 2.527 | 2.562 |
| 0.305 | 2.830 | 2.795 |
| 0.125 | 2.955 | 2.99 |
| 0.045 | 3 | No pin |

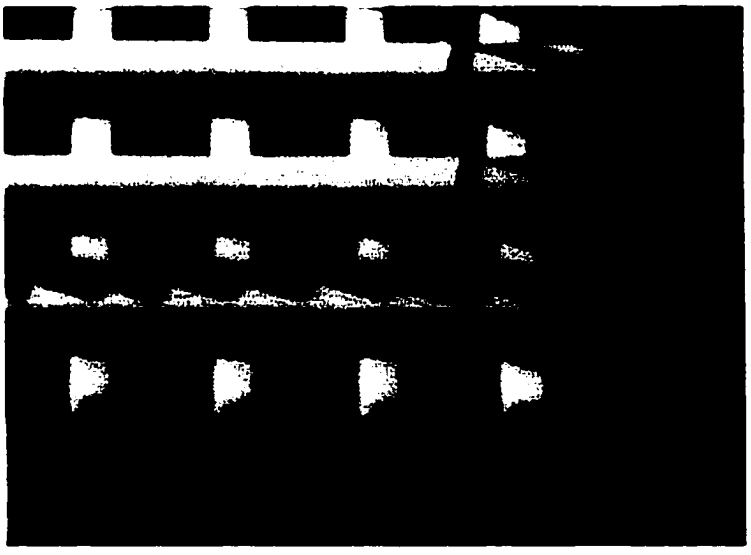

Figure A.1: Picture of the alignment jig in use. Ceramic rods are held in place with rolled pins. Once the rods are glued to each other the finished sheet can be taken out of the jig easily.

The loss and mode measurements required moving one probe. This was accomplished by mounting a spool onto the gear motor, and using it to wind up a metal measuring tape, the other end of which was connected to the probe (Figure 7.2). I choose a metal measuring tape for its stiffness. Unlike string, it will not stretch at the forces encountered in our setup.

**Index of Refraction Measurement**

Index of refraction was measured using a Fabry-Perot cavity. To do this a large number of rods were assembled into a block. This block was placed between a pair of metal horns (Figure A.2), and transmission was measured as a function of frequency.

Examining the resulting transmission response shown in Figure A.3 one notices sharp minima. The frequencies for which the minima are found can be related to the thickness *d* of the block, and the block's index of refraction *n*. $n = mc/2df$, where m is the number of wavelengths contained within the block.

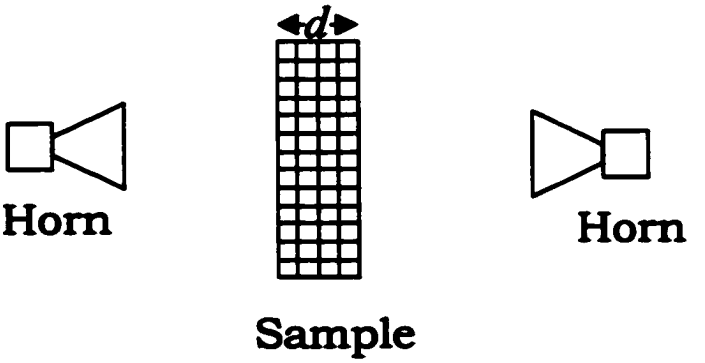


**Figure A.2: Fabry-Perot transmission measurements on a sample of closely packed rods are used to determine the index of refraction of the rods' ceramic material.**

This measurement was repeated for a second block thickness to find *m*. One can now calculate the index of refraction of the ceramic rods.

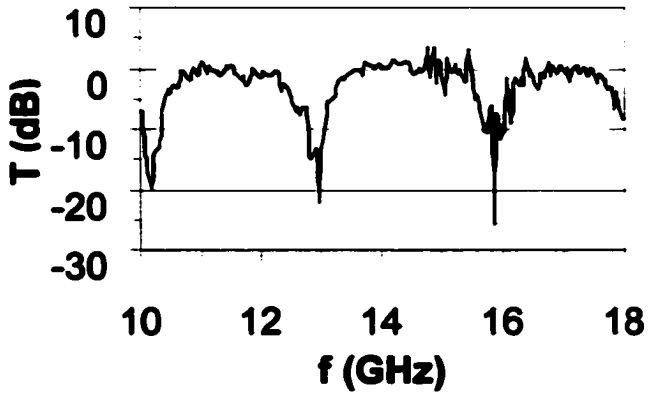


Figure A.3: Fabry-Perot transmission pattern produced by ceramic rods assembled into a 6-layer slab.

## REFERENCES

[1] E. Yablonovitch, "Inhibited Spontaneous Emission in Solid-State Physics and Electronics," Physics Review Letters, Volume 58, Number 20, pp. 2059-2062 (1987)

[2] Y. A. Vlasov, X. Z. Bo, J. C. Sturm, and D. J. Norris, "On-chip natural assembly of silicon photonic bandgap crystals," Nature, Volume 414, pp. 289-293 (2001)

[3] R. Guenther, Modern Optics, Wiley, New York, p. 83 (1990)

[4] J. A. Kong, Electromagnetic Wave Theory, EMW Publishing, Cambridge, p. 68 (1998)

[5] M. M. Sigalas, R. Biswas. K. M. Ho, C. M. Soukoulis, D. Turner, B. Vasiliu, S. C. Kothari, and Shawn Lin, "Waveguide Bends in Three-dimensional Layer-By-Layer Photonic Bandgap Materials," Microwave and Optical Technology Letters, Volume 23, Number 1, pp. 56-59 (1999)

[6]A. Chutinan and S. Noda, "Highly confined waveguides and waveguide bends in three-dimensional photonic crystal," Applied Physics Letters, Volume 75, Number 24, pp. 3739-3741 (1999)

[7] M. Bayindir, E. Ozbay, B. Temelkuran, M. M. Sigalas, C. M. Soukoulis, R. Biswas, and K. M. Ho, "Guiding, bending, and splitting of electromagnetic waves in highly confined photonic crystal waveguides," Physical Review B, Volume 63, R081107 (2001)

[8] J. P. Kavanaugh, "Photonic bandgap resonators and waveguides," Iowa State University, PhD. thesis (2001)

[9] R. C. McPhedran, N. A. Nicorovici, D. R. McKenzie, L. C. Botten, A. R. Parker, and G. W. Rouse, "The Sea Mouse and the Photonic Crystal," Australian Journal of Chemistry, Volume 54, pp. 241-244 (2001)

[10] E. Yablonovitch and T. J. Gmitter, "Photonic Band Structure: The Face-Centered-Cubic Case," Physics Review Letters, Volume 63, Number 18, pp. 1950-1953 (1989)

[11] K. M. Leung and Y. F. Liu, "Full Vector Wave Calculation of Photonic Band Structures in Face-Centered-Cubic Dielectric Media," Physics Review Letters, Volume 65, Number 21, pp. 2646-2649 (1990)

[12] Z. Zhang and S. Satpathy, "Electromagnetic Wave Propagation in Periodic Structures: Bloch Wave Solutions of Maxwell's Equations," Physics Revue Letters, Volume 65, Number 21, pp. 2650-2653 (1990)

[13] K. M. Ho, C. T. Chan, and C. M. Soukoulis, "Existence of a Photonic Gap in Periodic Dielectric Structures," Physics Review Letters, Volume 65, Number 25, pp. 3152-3155 (1990)

[14] J. Maddox, "Photonic bandgap crystals bite the dust," Nature, Volume 348, p. 481 (1990)

[15] E. Yablonovitch, T. J. Gmitter, and K. M. Leung, "Photonic Band Structure: The Face-Centered-Cubig Case employing nonspherical atoms," Physics Review Letters, Volume 67, Number17, pp. 2295-2298 (1991)

[16] K. M. Ho, C. T. Chan, C. M. Soukoulis, R. Biswas, and M. Sigalas, "Photonic Band Gaps in Three Dimensions: New Layer-By-Layer Periodic Structures," Solid State Communications, Volume 89, Number 5, pp. 413-416 (1994)

[17] S. Y. Lin, J. G. Fleming, D. L. Hetherington, B. K. Smith, R. Biswas, K. M. Ho, M. M. Sigalas, W. Zubrzycki, S. R. Kurtz, and Jim Bur, "A three-dimensional photonic crystal operating at infrared wavelengths," Nature, Volume 394, pp. 251-253 (1998)

[18] Susumu Noda, Katsuhiro Tomoda, Noritsugu Yamamoto, and Alongkarn Chutinan, "Full Three-Dimensional Photonic Bandgap Crystals at Near-Infrared Wavelengths," Science, Jul 28, pp. 604-606 (2000)

[19] Kanna Aoki, Hideki T. Miyazaki, Hideki Hirayama, Kioji Inoshita, Toshihiko Baba, Kazuaki Sakoda, Norio Shinya and Yoshinobu Aoyagi, "Microassembly of semiconductor three-dimensional photonic crystals," Nature Materials, Volume 2, pp. 117-121 (2003)

[20] T. Søndergaard, A. Bjarklev, M. Kristensen, J. Erland, and J. Broeng, "Designing finite-height two-dimensional photonic crystal waveguides," Applied Physics Letters, Volume 77, pp. 785-787 (2000)

[21] Z. Y. Li and K. M. Ho, "Waveguide network in three-dimensional layer-by-layer photonic crystals," Journal of the Optical Society of America B, Accepted for publication in May (2003)

[22] T. Baba, N. Fukaya, and A. Montegi, "Clear correspondence between theoretical and experimental light propagation characteristics in photonic crystal waveguides," Electronics Letters, Volume 37, Number 12, pp. 761-762 (2001)

[23] C. J. M. Smith, H. Benisty, S. Oliver, M. Rattier, C. Weisbuch, T. F. Krauss, R. M. De La Rue, R. Houdré, and U. Oesterle, "Low-loss channel waveguides with two-dimensional photonic crystal boundaries," Applied Physics Letters, Volume 77, Number 18, pp. 2813-2815 (2000)

[24] R. Guenther, Modern Optics, Wiley, New York, p. 255 (1990)

[25] H. P. Shuch, "Transmission Media," The ARRL UHF/Microwave Experimenters Manual, pp. 5.24 – 5.26 (1997)

[26] M. Loncar, D. Nedeljkovic, T. P. Pearsall, J. Vuckovic, A. Scherer, S. Kuchinsky, and D. C. Allan, "Experimental and theoretical confirmation of Bloch-mode light propagation in planar photonic crystal waveguides," Applied Physics Letters, Volume 80, Number 10, pp.1689-1691 (2002)

[27] S. Mingaleev and Y. Kivshar, "Non linear photonic crystals toward all-optical technologies," Optics and Photonics News, Volume 13, Number 7, pp. 48-51+62 (2002)